A space-time Energetic BIE method
for 3D Elastodynamics. The Dirichlet case.

Dear Author,

Here are the proofs of your article.

- You can submit your corrections **online**, via **e-mail** or by **fax**.
- For **online** submission please insert your corrections in the online correction form. Always indicate the line number to which the correction refers.
- You can also insert your corrections in the proof PDF and **email** the annotated PDF.
- For fax submission, please ensure that your corrections are clearly legible. Use a fine black pen and write the correction in the margin, not too close to the edge of the page.
- Remember to note the **journal title**, **article number**, and **your name** when sending your response via e-mail or fax.
- **Check** the metadata sheet to make sure that the header information, especially author names and the corresponding affiliations are correctly shown.
- **Check** the questions that may have arisen during copy editing and insert your answers/ corrections.
- **Check** that the text is complete and that all figures, tables and their legends are included. Also check the accuracy of special characters, equations, and electronic supplementary material if applicable. If necessary refer to the *Edited manuscript.*
- The publication of inaccurate data such as dosages and units can have serious consequences. Please take particular care that all such details are correct.
- Please **do not** make changes that involve only matters of style. We have generally introduced forms that follow the journal's style. Substantial changes in content, e.g., new results, corrected values, title and authorship are not allowed without the approval of the responsible editor. In such a case, please contact the Editorial Office and return his/her consent together with the proof.
- If we do not receive your corrections **within 48 hours**, we will send you a reminder.
- Your article will be published **Online First** approximately one week after receipt of your corrected proofs. This is the **official first publication** citable with the DOI. **Further changes are, therefore, not possible.**
- The **printed version** will follow in a forthcoming issue.

Please note

After online publication, subscribers (personal/institutional) to this journal will have access to the complete article via the DOI using the URL: http://dx.doi.org/[DOI].
If you would like to know when your article has been published online, take advantage of our free alert service. For registration and further information go to: http://www.link.springer.com.

Due to the electronic nature of the procedure, the manuscript and the original figures will only be returned to you on special request. When you return your corrections, please inform us if you would like to have these documents returned.

Metadata of the article that will be visualized in OnlineFirst

ArticleTitle	A space–time energetic BIE method for 3D elastodynamics: the Dirichlet case	
Article Sub-Title		
Article CopyRight	The Author(s), under exclusive licence to Springer-Verlag GmbH Germany, part of Springer Nature (This will be the copyright line in the final PDF)	
Journal Name	Computational Mechanics	
Corresponding Author	FamilyName	**Desiderio**
	Particle	
	Given Name	**L.**
	Suffix	
	Division	Department of Mathematical, Physical and Computer Sciences
	Organization	University of Parma
	Address	Parma, Italy
	Phone	
	Fax	
	Email	luca.desiderio@unipr.it
	URL	
	ORCID	http://orcid.org/0000-0002-3924-0939
Author	FamilyName	**Aimi**
	Particle	
	Given Name	**A.**
	Suffix	
	Division	Department of Mathematical, Physical and Computer Sciences
	Organization	University of Parma
	Address	Parma, Italy
	Phone	
	Fax	
	Email	
	URL	
	ORCID	
Author	FamilyName	**Dallospedale**
	Particle	
	Given Name	**S.**
	Suffix	
	Division	Department of Sciences and Methods for Engineering
	Organization	University of Modena
	Address	Modena, Italy
	Phone	
	Fax	
	Email	
	URL	
	ORCID	
Author	FamilyName	**Guardasoni**
	Particle	
	Given Name	**C.**
	Suffix	
	Division	Department of Mathematical, Physical and Computer Sciences
	Organization	University of Parma
	Address	Parma, Italy
	Phone	
	Fax	
	Email	
	URL	
	ORCID	

Schedule	Received Revised Accepted	26 Oct 2022 1 Mar 2023

Abstract	We consider the retarded potential boundary integral equation, arising from the 3D elastic (vector) wave equation problem, endowed with a Dirichlet condition on the boundary and null initial conditions. For its numerical solution, we employ a weak formulation related to the energy of the system and we discretize it by a Galerkin-type boundary element method (BEM). This approach, called energetic BEM, has been already applied in the context of time-domain acoustic (scalar) wave propagation and it has revealed accurate and stable even on large time intervals of analysis. In particular, when standard (constant) shape functions for time discretization are employed, the double integration in time can be performed analytically. Then, one is left with the task of evaluating double space integrals, whose integration domains are generally delimited by the wave fronts of the primary and the secondary waves. Since the accurate computation of the integrals involved in the numerical scheme is a key issue for the stability of the method, we propose an efficient evaluation strategy, based on the exact detection of the integration domain. The presented numerical tests show the effectiveness of the proposed approach.

Keywords (separated by '-')	3D elastodynamics - Space–time boundary integral equations - Energetic boundary element method
Footnote Information	A. Aimi, L. Desiderio and C. Guardasoni: Members of the INdAM-GNCS Research Group, Italy.

Computational Mechanics
https://doi.org/10.1007/s00466-023-02312-z

ORIGINAL PAPER

A space–time energetic BIE method for 3D elastodynamics: the Dirichlet case

A. Aimi[1] · S. Dallospedale[2] · L. Desiderio[1] · C. Guardasoni[1]

Received: 26 October 2022 / Accepted: 1 March 2023

Abstract

We consider the retarded potential boundary integral equation, arising from the 3D elastic (vector) wave equation problem, endowed with a Dirichlet condition on the boundary and null initial conditions. For its numerical solution, we employ a weak formulation related to the energy of the system and we discretize it by a Galerkin-type boundary element method (BEM). This approach, called energetic BEM, has been already applied in the context of time-domain acoustic (scalar) wave propagation and it has revealed accurate and stable even on large time intervals of analysis. In particular, when standard (constant) shape functions for time discretization are employed, the double integration in time can be performed analytically. Then, one is left with the task of evaluating double space integrals, whose integration domains are generally delimited by the wave fronts of the primary and the secondary waves. Since the accurate computation of the integrals involved in the numerical scheme is a key issue for the stability of the method, we propose an efficient evaluation strategy, based on the exact detection of the integration domain. The presented numerical tests show the effectiveness of the proposed approach.

Keywords 3D elastodynamics · Space–time boundary integral equations · Energetic boundary element method

1 Introduction

The design of a suitable, efficient and accurate numerical method to solve elastodynamic problems is encountered in many academic and industrial applications. To cite a few examples: the development of a powerful forward engine in the framework of Full-Waveform Inversion (FWI) for the estimation of the elastic parameters in the underground; the study of fluid–structure interactions; the numerical solution of contact problems. Even if different directions exist, the use of a boundary integral equation (BIE) technique, whose discretization is known as the boundary element method (BEM), is an appealing choice because it allows to handle problems defined on the exterior of bounded domains as easily as those defined in the interior, without the introduction of an artificial boundary to truncate the computational domain. Furthermore, this technique requires the discretization only of the domain boundaries, leading to a drastic reduction of the total number of degrees of freedom of the problem. To simulate elastic wave propagation, most BEMs assume time invariant harmonic excitation so that the unknowns are time invariant complex fields. Even if this analysis has been used for many years by engineers, the transient behaviour witnessed in the real world may only be recovered by calculation of many frequency-domain models and inverse discrete Fourier transform. Unfortunately, solving one frequency-domain BEM equation in a 3D domain is computationally very costly, since the resulting linear system is fully-populated, so that acceleration techniques have to be employed in order to obtain accurate solutions in reasonable computational times. Most of them are based on the compression of the system matrix aiming at applying efficient direct or iterative solvers (see e.g. hierarchical matrices [9, 16, 19] and fast multiple methods [35]).

An alternative is to drop the time invariant assumption and formulate the transient problems in the time-domain, which is usually called Time-Domain BEMs (TD-BEMs). As well summarized in [24, 30], the discretization of TD-BIEs by collocation methods has some advantages in implementation

A. Aimi, L. Desiderio and C. Guardasoni: Members of the INdAM-GNCS Research Group, Italy.

✉ L. Desiderio
luca.desiderio@unipr.it

1 Department of Mathematical, Physical and Computer Sciences, University of Parma, Parma, Italy

2 Department of Sciences and Methods for Engineering, University of Modena, Modena, Italy

due to its simplicity but gives rise to instability issues (see e.g. [23, 34]), avoided by some variational approaches as well as by convolution quadrature methods [27], but these latter with some drawbacks highlighted in [13].

Among the variational approaches, as the one theoretically analyzed in the milestone paper [14], a Galerkin TD-BEM for the discretization of the BIEs related to acoustic (scalar) wave propagation problems has been introduced in [2]. The proposed technique is based on a natural energy identity satisfied by the solution of the corresponding differential problem, which leads to a space–time weak formulation of the BIEs with precise continuity and coerciveness properties (see [3]). Consequently, the integral problem can be discretized by unconditionally stable schemes with well-behaved stability constants even for large times [4]. The algebraic reformulation of the energetic BEM (EBEM) leads to a linear system whose matrix has a Toeplitz lower-triangular block structure, that allows the acceleration of the solution phase. As a direct consequence of the flexibility of the EBEM, a large body of literature has risen to witness its capabilities to simulate 3D acoustic (see [5]) and 2D elastodynamic (see [8, 10–12]) wave propagation in semi-infinite or infinite media. Furthermore, we recall that the energetic space–time BIEs, hence the associated potential representations, have been also used to restrict the original partial differential equation (PDE) exterior acoustic problem to a bounded region of physical interest. Indeed, this approach has allowed to construct transparent (or non-reflecting) boundary conditions on the boundary of the chosen region and to retrive the solution of the original problem in the new exterior bounded domain by using the Finite Element Method (see [6, 7]).

In this paper, we extend the EBEM to 3D elastodynamic problems, showing the capabilities of the method of modelling a full wavefield rather than specific wave types and addressing various computational aspects of the proposed approximation method. In particular, we consider the Navier–Cauchy equation of motion, defined in bounded or unbounded domains external to 3D obstacles and endowed with a Dirichlet condition on the boundary and null initial conditions. Such problems are reformulated in terms of a space–time weakly-singular BIE of the first kind, whose energetic full space–time discretization requires double integration both in space and in time. Since a key ingredient for the success of the EBEM is the efficient and accurate evaluation of all the involved integrals, the selected formulation could be quite challenging in large scale applications. Nevertheless, if standard (constant) shape functions for time discretization are employed, the double integration in time can be performed analytically and one is left with the task of evaluating double space integrals, whose integration domains are generally delimited by the wave fronts of the primary and the secondary waves. In order to exactly detect this latter, and consequently to preserve the stability properties of the EBEM, we choose boundary meshes made by triangular elements with straight sides and we propose an ad-hoc numerical integration scheme, tailored for the correct domain of integration. We remark that such a study has been presented in [5] in the case of 3D acoustic (scalar) wave equation but a straightforward generalization to elastic (vector) problems is not possible, due to a more involved fundamental solution and the presence of two wave fronts.

The paper is organized as follows: after presenting the model problem in the next section, we recall its energetic BIE weak formulation in Sect. 3. Then, we devote Sect. 4 to detail the energetic BEM discretization, focusing on its algebraic reformulation and on the analysis of the time-integrated kernels generating the matrix entries. In Sect. 5, we describe the numerical and analytical strategies adopted for the double space integrals at hand, with a specific attention devoted to the representation of the wave fronts of the primary and secondary waves. Numerical results validating the proposed approach are illustrated and discussed in Sect. 6. Finally, some conclusions are drawn in the last section.

2 Model problem

In the Euclidean space $\mathbf{R}^3$ equipped with a fixed orthonormal Cartesian coordinates axes $\mathbf{e}_1, \mathbf{e}_2, \mathbf{e}_3$ with origin at $\mathbf{O} = (0, 0, 0)^\top$, let $\Omega_l \subset \mathbf{R}^3$ be a domain admitting a connected, smooth and orientable closed boundary surface $\Gamma = \partial\Omega_l$. In absence of body forces, we are interested in studying the propagation of elastic waves in a homogeneous isotropic elastic medium occupying Ω_l. When the domain is a finite volume the problem is interior with using the notation $l = i$. Otherwise, it is set $l = e$ and we study the exterior problem. Moreover, let $\Omega = \Omega_i \cup \Omega_e = \mathbf{R}^3 \setminus \Gamma$.

In both Ω_l, $l = i, e$, assuming small variations of the (real-valued) displacement field $\mathbf{u}(\mathbf{x}; t) = (u_1, u_2, u_3)^\top$ at location $\mathbf{x} = (x_1, x_2, x_3)^\top \in \Omega_l$ and time $t \in [0, T]$, this latter is defined by the following system:

$$\varrho\ddot{\mathbf{u}}(\mathbf{x}; t) - \mu\boldsymbol{\Delta}\mathbf{u}(\mathbf{x}; t) - (\lambda + \mu)\boldsymbol{\nabla}\boldsymbol{\nabla}\cdot\mathbf{u}(\mathbf{x}; t) = \mathbf{0} \qquad (\mathbf{x}; t) \in \Omega_l \times [0, T] \tag{2.1a}$$

$$\mathbf{u}(\mathbf{x}; t) = \mathbf{g}(\mathbf{x}; t) \qquad (\mathbf{x}; t) \in \Gamma \times [0, T] \tag{2.1b}$$

$$\mathbf{u}(\mathbf{x}; 0) = \mathbf{0} \qquad \mathbf{x} \in \Omega_l \tag{2.1c}$$

$$\dot{\mathbf{u}}(\mathbf{x}; 0) = \mathbf{0} \qquad \mathbf{x} \in \Omega_l \tag{2.1d}$$

where ϱ is the mass density, μ is the shear modulus and λ is the Lamé parameter. These last two quantities are related to the Poisson ratio ν by $\lambda := 2\mu\nu(1-2\nu)^{-1}$. Furthermore, the

Journal: 466 MS: 2312 TYPESET DISK LE CP Disp.:2023/3/30 Pages: 21 Layout: Large

superposed dot indicates time differentiation, while ∇ and $\boldsymbol{\Delta}$ denote the nabla and the Laplace operators, respectively.
In the above problem, Eq. (2.1a) is known as Navier–Cauchy equation of motion, Eq. (2.1b) represents a boundary condition of Dirichlet type with datum $\mathbf{g}(\mathbf{x};t)$ and Eqs. (2.1c) and (2.1d) are the quiescent initial conditions, that specify the value of $\mathbf{u}(\mathbf{x};t)$ and $\dot{\mathbf{u}}(\mathbf{x};t)$ at the first time of interest $t=0$.
Elastodynamics waves are characterized by primary and secondary velocities, defined by $c_\mathrm{P}^2 := (\lambda+2\mu)\varrho^{-1}$, $c_\mathrm{S}^2 := \mu\varrho^{-1}$ and related, respectively, to the so-called primary or pressure waves (P-waves in short) and secondary or shear waves (S-waves in short). Since for any real materials $-1 < \nu < 0.5$, it's easy to verify that $c_\mathrm{P} > c_\mathrm{S}$, that is P-waves travel faster than S-waves.
In what follows, we denote by $\boldsymbol{\sigma}[\mathbf{u}](\mathbf{x};t)$ and $\boldsymbol{\epsilon}[\mathbf{u}](\mathbf{x};t)$ the second order stress and strain tensors, respectively. The latter is defined by the constitutive law of the linear elastic model, i.e.

$$\boldsymbol{\epsilon}[\mathbf{u}](\mathbf{x};t) = \frac{1}{2}\left[\nabla\mathbf{u}(\mathbf{x};t) + \nabla\mathbf{u}(\mathbf{x};t)^\top\right] \tag{2.2}$$

and it is related to the stress tensor through the Hooke's law

$$\boldsymbol{\sigma}[\mathbf{u}](\mathbf{x};t) = \boldsymbol{C} : \boldsymbol{\epsilon}[\mathbf{u}](\mathbf{x};t), \tag{2.3}$$

in which the symbol ":" denotes the double tensor inner product and $\boldsymbol{C}$ is the fourth order relaxation tensor, whose components are given by $C_{ij}^{k\ell} := \lambda\delta_{ij}\delta_{k\ell} + \mu\left(\delta_{ik}\delta_{j\ell} + \delta_{i\ell}\delta_{jk}\right)$ for $i,j,k,\ell = 1,2,3$ (δ_{ij} being the Kronecker symbol).
Furthermore, the traction vector $\mathbf{p} = (p_1,p_2,p_3)^\top$ along Γ can be defined through the stress tensor as:

$$\mathbf{p}(\mathbf{x};t) := \boldsymbol{\sigma}[\mathbf{u}](\mathbf{x};t)\cdot\mathbf{n}, \tag{2.4}$$

where $\mathbf{n}$ denotes the unit normal vector to the boundary pointing outside the domain Ω_l.

3 Energetic TD-BIE weak formulation

It is well known that, starting from the Somigliana identity (see [15]) written for both Ω_i and Ω_e, the solution of the initial boundary value problem (2.1) can be represented as single-layer potential (see [18]), i.e.

$$\mathbf{u}(\mathbf{x};t) := \int_0^t\int_\Gamma \mathbf{G}(\mathbf{x},\mathbf{y};t,\tau)\mathbf{w}(\mathbf{y};\tau)\mathrm{d}\Gamma_\mathbf{y}\mathrm{d}\tau, \qquad \mathbf{x}\in\Omega_l \quad \text{and} \quad t\in[0,T], \tag{3.1}$$

where $\mathbf{w} = (w_1,w_2,w_3)^\top$ is a suitable density field to be determined in the same functional space of the traction field $\mathbf{p}$. Furthermore, the second-order tensor $\mathbf{G}$ satisfies the Green's identity in relation to Navier–Cauchy operator in the left hand side of Equation (2.1a). Hence, it is the fundamental solution of the equation

$$\varrho\ddot{\mathbf{u}}(\mathbf{x};t) - \mu\boldsymbol{\Delta}\mathbf{u}(\mathbf{x};t) - (\lambda+\mu)\nabla\nabla\cdot\mathbf{u}(\mathbf{x};t) = \delta(\mathbf{x}-\mathbf{y})\delta(t-\tau)\mathbf{I}, \tag{3.2}$$

where $\mathbf{I}$ stands for the 3-by-3 identity tensor, and it represents the response at the observation point $\mathbf{x}$ and observation time t due to a unit magnitude load, modelled by the Dirac distribution $\delta(\cdot)$ and acting at the source point $\mathbf{y}$ and emission time τ. Since the coefficients in (2.1a) are independent of space and time, the components of the tensor $\mathbf{G}$ depend on the arguments $\mathbf{x},\mathbf{y},t,\tau$ only through the differences $\mathbf{r} := \mathbf{x}-\mathbf{y}$ and $t-\tau$, i.e. for $i,j=1,2,3$ (see [15])

$$\begin{aligned} G_{ij}(\mathbf{x},\mathbf{y};t,\tau) &:= \frac{1}{4\pi\varrho c_\mathrm{P}^2}\frac{r_ir_j}{r^3}\delta\left(t-\tau-\frac{r}{c_\mathrm{P}}\right) \\ &+ \frac{1}{4\pi\varrho c_\mathrm{S}^2}\left(\frac{\delta_{ij}}{r}-\frac{r_ir_j}{r^3}\right)\delta\left(t-\tau-\frac{r}{c_\mathrm{S}}\right) \\ &- \frac{1}{4\pi\varrho}\left(\frac{\delta_{ij}}{r^3}-\frac{r_ir_j}{r^5}\right)(t-\tau) \\ &\left[H\left(t-\tau-\frac{r}{c_\mathrm{P}}\right) - H\left(t-\tau-\frac{r}{c_\mathrm{S}}\right)\right], \end{aligned} \tag{3.3}$$

where r_i is the i-th component of $\mathbf{r}$, the distance $r := |\mathbf{x}-\mathbf{y}|$ is the euclidean norm of $\mathbf{r}$ and $H(\cdot)$ is the Heaviside function. We remark that the expression (3.3) can be recast in the following form:

$$\begin{aligned} G_{ij}(\mathbf{x},\mathbf{y};t,\tau) &= \frac{r_ir_j}{r^2}G_\mathrm{P}(\mathbf{x},\mathbf{y};t,\tau) \\ &+ \left(\delta_{ij}-\frac{r_ir_j}{r^2}\right)G_\mathrm{S}(\mathbf{x},\mathbf{y};t,\tau) \\ &- \left(\delta_{ij}-3\frac{r_ir_j}{r^2}\right)\left[\widetilde{G}_\mathrm{P}(\mathbf{x},\mathbf{y};t,\tau)\right. \\ &\left.-\widetilde{G}_\mathrm{S}(\mathbf{x},\mathbf{y};t,\tau)\right], \end{aligned} \tag{3.4}$$

in which

$$G_*(\mathbf{x},\mathbf{y};t,\tau) := \frac{1}{4\pi\varrho c_*^2 r}\delta\left(t-\tau-\frac{r}{c_*}\right) \quad \text{with } * = P,S \tag{3.5}$$

is the fundamental solution for the 3D scalar wave equation, while $\widetilde{G}_*(\mathbf{x},\mathbf{y};t,\tau)$ is defined by

$$\widetilde{G}_*(\mathbf{x},\mathbf{y};t,\tau) := \frac{1}{4\pi\varrho r^3}(t-\tau)H\left(t-\tau-\frac{r}{c_*}\right) \quad \text{with } * = P,S. \tag{3.6}$$

Journal: 466 MS: 2312 TYPESET DISK LE CP Disp.:2023/3/30 Pages: 21 Layout: Large

From (3.1), with a limiting process that makes a point $\mathbf{x} \in \Omega_l$ tending to a point $\mathbf{x} \in \Gamma$ and exploiting the Dirichlet boundary condition, we can obtain a system of three TD-BIEs:

$$\int_0^t \int_\Gamma \mathbf{G}(\mathbf{x}, \mathbf{y}; t, \tau)\mathbf{w}(\mathbf{y}; \tau) d\Gamma_{\mathbf{y}} d\tau = \mathbf{g}(\mathbf{x}; t),$$
$$(\mathbf{x}; t) \in \Gamma \times [0, T]. \tag{3.7}$$

For $s \in [-1, 1]$, let $H^s(\Gamma)$ denote the usual fractional order Sobolev space, with $H^0(\Gamma) = L^2(\Gamma)$, and $\mathbf{H}^s(\Gamma) = (H^s(\Gamma))^3$. Referring to [10, 17, 30] for what concerns the following functional spaces, introducing the space–time integral operator $\mathbf{V} : L^2\left([0, T]; \mathbf{H}^{-1/2}(\Gamma)\right) \to H^1\left([0, T]; \mathbf{H}^{1/2}(\Gamma)\right)$ such that:

$$\mathbf{V}\left[\mathbf{w}\right](\mathbf{x}; t) := \int_0^t \int_\Gamma \mathbf{G}(\mathbf{x}, \mathbf{y}; t, \tau)\mathbf{w}(\mathbf{y}; \tau) d\Gamma_{\mathbf{y}} d\tau,$$
$$(\mathbf{x}; t) \in \Gamma \times [0, T], \tag{3.8}$$

the TD-BIEs (3.7) can be written with the compact notation

$$\mathbf{V}\left[\mathbf{w}\right](\mathbf{x}; t) = \mathbf{g}(\mathbf{x}; t),$$
$$(\mathbf{x}; t) \in \Gamma \times [0, T]. \tag{3.9}$$

The above BIE will be set in the so-called energetic weak form. With this aim, following what has been proven in [11] for 2D elastodynamics, which can be straightforwardy extended to 3D space dimension, we introduce the energy of the Navier–Cauchy equation (2.1a), which is defined as follows:

$$\mathcal{K}(t; \mathbf{u}) := \frac{1}{2} \int_\Omega \varrho \left|\dot{\mathbf{u}}(\mathbf{x}; t)\right|^2 d\mathbf{x}$$
$$+ \frac{1}{2} \int_\Omega \boldsymbol{\sigma}[\mathbf{u}](\mathbf{x}; t) : \boldsymbol{\epsilon}[\mathbf{u}](\mathbf{x}; t) d\mathbf{x} \tag{3.10}$$

and we remark that the solution $\mathbf{u}$ of problem (2.1) satisfies the following energy identity

$$\mathcal{K}(T; \mathbf{u}) = \int_0^T \int_\Gamma \mathbf{w}^\top(\mathbf{x}; t)\dot{\mathbf{u}}(\mathbf{x}; t) d\Gamma_{\mathbf{x}} dt. \tag{3.11}$$

which can be obtained multiplying equation (2.1a) by $\dot{\mathbf{u}}$ and integrating by parts over $\Omega \times [0, T]$.

Having introduced the bilinear form $\mathcal{A}_{\mathcal{K}} : L^2\left([0, T]; \mathbf{H}^{-1/2}(\Gamma)\right) \times L^2\left([0, T]; \mathbf{H}^{-1/2}(\Gamma)\right) \to \mathbf{R}$ defined by

$$\mathcal{A}_{\mathcal{K}}(\mathbf{w}, \mathbf{v}) := \int_0^T \int_\Gamma \mathbf{v}^\top(\mathbf{x}; t) \frac{\partial}{\partial t} \mathbf{V}[\mathbf{w}](\mathbf{x}; t) d\Gamma_{\mathbf{x}} dt, \tag{3.12}$$

the space–time energetic weak formulation of the TD-BIEs (3.9) reads as follows

find the density function $\mathbf{w} \in L^2\left([0, T]; \mathbf{H}^{-1/2}(\Gamma)\right)$ *such that:*

$$\mathcal{A}_{\mathcal{K}}(\mathbf{w}, \mathbf{v}) = \int_0^T \int_\Gamma \mathbf{v}^\top(\mathbf{x}; t)\dot{\mathbf{g}}(\mathbf{x}; t) d\Gamma_{\mathbf{x}} dt$$
$$\forall \mathbf{v} \in L^2\left([0, T]; \mathbf{H}^{-1/2}(\Gamma)\right). \tag{3.13}$$

Note that $\mathcal{A}_{\mathcal{K}}$ is defined as a quadruple integral, double in space and double in time.

The above weak BIEs system is the core of the entire method: its numerical resolution generates an approximation of vector field $\mathbf{w}$ that can be used in the representation formula (3.1), recovering in a post-processing phase the behaviour of the displacement $\mathbf{u}$ at each point of the space domain and at each time instant.

4 Galerkin BEM discretization

For the discretization phase, we consider a uniform decomposition of the time interval $[0, T]$ with time step $\Delta_t := T/N_{\Delta_t}$, N_{Δ_t} being a positive integer, generated by $N_{\Delta_t} + 1$ instants:

$$t_n := n\Delta_t, \qquad n = 0, \ldots, N_{\Delta_t} \tag{4.1}$$

and we choose temporally piecewise constant shape functions, although higher degree shape functions can be used. Note that, for this particular choice, the shape functions, denoted by $\bar{v}_n(t)$, are defined as:

$$\bar{v}_n(t) := H(t - t_n) - H(t - t_{n+1}),$$
$$n = 0, \ldots, N_{\Delta_t} - 1. \tag{4.2}$$

For the space discretization, we introduce on Γ an admissible triangulation $\mathcal{T}_{\Delta_{\mathbf{x}}}(\Gamma) := \{E_1, \ldots, E_{M_{\Delta_{\mathbf{x}}}}\}$ constituted by $M_{\Delta_{\mathbf{x}}}$ flat triangular elements. The index $\Delta_{\mathbf{x}}$ denotes the mesh size. We also assume that $\cup_{i=1}^{M_{\Delta_{\mathbf{x}}}} E_i$ coincides with $\overline{\Gamma}$ if the boundary is polygonal, or it is a suitable approximation of $\overline{\Gamma}$, otherwise. The functional background compels one to choose spatially shape functions whose components belong

Journal: 466 MS: 2312 TYPESET DISK LE CP Disp.:2023/3/30 Pages: 21 Layout: Large

to $L^2(\Gamma)$. Hence, we consider piecewise constant basis functions $v_m(\mathbf{x})$, $m = 1, \ldots, M_{\Delta_x}$ related to $\mathcal{T}_{\Delta_x}(\Gamma)$. Thus, the approximate solution of (3.13) is expressed as:

$$\mathbf{w}(\mathbf{x};t) \simeq \widetilde{\mathbf{w}}(\mathbf{x};t) := \sum_{n=0}^{N_{\Delta_t}-1} \bar{v}_n(t) \sum_{m=1}^{M_{\Delta_x}} \boldsymbol{\alpha}_m^{(n)} v_m(\mathbf{x})$$
$$\text{with} \quad \boldsymbol{\alpha}_m^{(n)} := \left(\alpha_{m,1}^{(n)}, \alpha_{m,2}^{(n)}, \alpha_{m,3}^{(n)}\right)^\top \tag{4.3}$$

and the test functions are replaced by

$$\mathbf{v}(\mathbf{x};t) = v_{\tilde{m}}(\mathbf{x})\bar{v}_{\tilde{n}}(t)\mathbf{e}, \tag{4.4}$$

where $\mathbf{e} := \mathbf{e}_1 + \mathbf{e}_2 + \mathbf{e}_3 = (1,1,1)^\top$. The Galerkin BEM discretization coming from the energetic weak formulation (3.13) produces the linear system

$$\mathbb{E}\boldsymbol{\alpha} = \boldsymbol{\beta}, \tag{4.5}$$

where the matrix $\mathbb{E}$ has a block lower triangular Toeplitz structure, since its elements depend on the difference $\Delta_{\tilde{n},n} := t_{\tilde{n}} - t_n$, and in particular they vanish if $t_{\tilde{n}} < t_n$. Since we deal with 3D elastodynamic problems, if we denote by $\mathbb{E}^{(\ell)}$ the block obtained when $\Delta_{\tilde{n},n} = \ell\Delta_t$, $\ell = 0, \ldots, N_{\Delta_t} - 1$, we remark that each pair of spatial indices $\tilde{m}, m = 1, \ldots, M_{\Delta_x}$ does not define a single entry of $\mathbb{E}^{(\ell)}$ but rather a 3×3 sub-block $\mathbb{E}_{\tilde{m},m}^{(\ell)}$. Thus, each block $\mathbb{E}^{(\ell)}$ of the matrix $\mathbb{E}$ requires $O\left((3M_{\Delta_x})^2\right)$ memory and computation time. Furthermore, the evaluation of a single entry of $\mathbb{E}_{\tilde{m},m}^{(\ell)}$ is expensive, because we have to address the issue of computing quadruple integrals:

$$\begin{aligned}
&\left(\mathbb{E}_{\tilde{m},m}^{(\ell)}\right)_{ij} \\
&= \int_0^T \int_\Gamma \frac{\partial}{\partial t}\left(\int_0^t \int_\Gamma G_{ij}(\mathbf{x},\mathbf{y};t,\tau) v_m(\mathbf{y})\bar{v}_n(\tau)\,d\Gamma_{\mathbf{y}}\,d\tau\right) \\
&\quad v_{\tilde{m}}(\mathbf{x})\bar{v}_{\tilde{n}}(t)\,d\Gamma_{\mathbf{x}}\,dt \\
&= -\int_0^T \int_\Gamma \left(\int_0^t \int_\Gamma G_{ij}(\mathbf{x},\mathbf{y};t,\tau) v_m(\mathbf{y})\bar{v}_n(\tau)\,d\Gamma_{\mathbf{y}}\,d\tau\right) \\
&\quad v_{\tilde{m}}(\mathbf{x})\dot{\bar{v}}_{\tilde{n}}(t)\,d\Gamma_{\mathbf{x}}\,dt
\end{aligned} \tag{4.6}$$

but, after a double analytic integration in the time variables, we obtain:

$$\begin{aligned}
\mathbb{E}_{\tilde{m},m}^{(\ell)} &= -\frac{1}{4\pi\varrho} \sum_{\eta,\tilde{\eta}=0}^{1} (-1)^{\eta+\tilde{\eta}} \int_{E_{\tilde{m}}} \int_{E_m} \mathbb{G}(\mathbf{x},\mathbf{y};\Delta_{\tilde{n}+\tilde{\eta},n+\eta}) \\
&\quad v_m(\mathbf{y}) v_{\tilde{m}}(\mathbf{x})\,d\Gamma_{\mathbf{y}}\,d\Gamma_{\mathbf{x}}.
\end{aligned} \tag{4.7}$$

In the above relationship, the components of the time-integrated kernel $\mathbb{G}$ are given by

$$\begin{aligned}
\mathbb{G}_{ij}(\mathbf{x},\mathbf{y};\Delta_{\tilde{n},n}) &= \frac{1}{c_P^2}\frac{r_i r_j}{r^3} H\left(\Delta_{\tilde{n},n} - \frac{r}{c_P}\right) \\
&+ \frac{1}{c_S^2}\left(\frac{\delta_{ij}}{r} - \frac{r_i r_j}{r^3}\right) H\left(\Delta_{\tilde{n},n} - \frac{r}{c_S}\right) - \frac{1}{2}\left(\frac{\delta_{ij}}{r^3} - \frac{r_i r_j}{r^5}\right) \\
&\left[\left(\Delta_{\tilde{n},n}^2 - \frac{r^2}{c_P^2}\right) H\left(\Delta_{\tilde{n},n} - \frac{r}{c_P}\right)\right. \\
&\left. - \left(\Delta_{\tilde{n},n}^2 - \frac{r^2}{c_S^2}\right) H\left(\Delta_{\tilde{n},n} - \frac{r}{c_S}\right)\right]
\end{aligned} \tag{4.8}$$

where the Heaviside functions represent the wave front propagation and their contribution is 0 or 1. If $r < c_S\Delta_{\tilde{n},n} < c_P\Delta_{\tilde{n},n}$, then (4.8) reduces to

$$\begin{aligned}
&\mathbb{G}_{ij}(\mathbf{x},\mathbf{y};\Delta_{\tilde{n},n}) \\
&= \frac{1}{2}\left(\frac{r_i r_j}{r^3}\frac{c_P^2 - c_S^2}{c_P^2 c_S^2} + \frac{\delta_{ij}}{r}\frac{c_P^2 + c_S^2}{c_P^2 c_S^2}\right)
\end{aligned} \tag{4.9}$$

and we observe a space singularity of type $\mathcal{O}(^1/_r)$ as $r \to 0$, which is typical of weakly singular kernels related to 3D elliptic problems. Moreover, when $0 < c_S\Delta_{\tilde{n},n} < r < c_P\Delta_{\tilde{n},n}$, (4.8) is no longer singular and becomes

$$\begin{aligned}
&\mathbb{G}_{ij}(\mathbf{x},\mathbf{y};\Delta_{\tilde{n},n}) \\
&= \frac{1}{2}\left(\frac{1}{c_P^2}\frac{\delta_{ij}}{r} - \frac{1}{c_P^2}\frac{r_i r_j}{r^3} - \frac{\delta_{ij}}{r^3}\Delta_{\tilde{n},n}^2 + 3\frac{r_i r_j}{r^5}\Delta_{\tilde{n},n}^2\right).
\end{aligned} \tag{4.10}$$

Combining (4.7) and (4.9), it easy to show that, if N^* denotes the first time index such that $c_P t_{N^*-1} > c_S t_{N^*-1} > \mathrm{diam}(\Gamma)$, we have $\mathbb{E}_{\tilde{m},m}^{(\ell)} = 0$ for all $\ell = N^*, \ldots, N_{\Delta_t-1}$. Due to this cut-off property, the matrix of the final linear system (4.5) has the well known band structure of standard collocation approaches [28], i.e.

Journal: 466 MS: 2312 TYPESET DISK LE CP Disp.:2023/3/30 Pages: 21 Layout: Large

$$
\begin{pmatrix}
\mathbb{E}^{(0)} & 0 & 0 & 0 & 0 & 0 & 0 & \dots & 0 \\
\mathbb{E}^{(1)} & \mathbb{E}^{(0)} & 0 & 0 & 0 & 0 & 0 & \dots & 0 \\
\mathbb{E}^{(2)} & \mathbb{E}^{(1)} & \mathbb{E}^{(0)} & 0 & 0 & 0 & 0 & \dots & 0 \\
\vdots & \vdots & \vdots & \ddots & \ddots & \vdots & \vdots & \vdots & \vdots \\
\mathbb{E}^{(N^*-1)} & \mathbb{E}^{(N^*-2)} & \mathbb{E}^{(N^*-3)} & \dots & \mathbb{E}^{(0)} & 0 & 0 & \dots & 0 \\
0 & \mathbb{E}^{(N^*-1)} & \mathbb{E}^{(N^*-2)} & \mathbb{E}^{(N^*-3)} & \dots & \mathbb{E}^{(0)} & 0 & \dots & 0 \\
0 & 0 & \mathbb{E}^{(N^*-1)} & \mathbb{E}^{(N^*-2)} & \mathbb{E}^{(N^*-3)} & \dots & \mathbb{E}^{(0)} & \dots & 0 \\
\vdots & \vdots & \ddots & \ddots & \ddots & \ddots & \dots & \ddots & \vdots \\
0 & 0 & \dots & 0 & \mathbb{E}^{(N^*-1)} & \mathbb{E}^{(N^*-2)} & \mathbb{E}^{(N^*-3)} & \dots & \mathbb{E}^{(0)}
\end{pmatrix}
\tag{4.11}
$$

while the unknowns and right hand side entries are organized as follows

$$
\begin{aligned}
\boldsymbol{\alpha} &= \left(\boldsymbol{\alpha}^{(0)}, \boldsymbol{\alpha}^{(1)}, \dots, \boldsymbol{\alpha}^{(N^*)}, \dots, \boldsymbol{\alpha}^{(N_{\Delta_t}-1)}\right)^\top \\
&\quad \text{with} \quad \boldsymbol{\alpha}^{(\ell)} = \left(\boldsymbol{\alpha}_1^{(\ell)}, \boldsymbol{\alpha}_2^{(\ell)}, \dots, \boldsymbol{\alpha}_{M_{\Delta_\mathrm{x}}}^{(\ell)}\right)^\top \\
\boldsymbol{\beta} &= \left(\boldsymbol{\beta}^{(0)}, \boldsymbol{\beta}^{(1)}, \dots, \boldsymbol{\beta}^{(N^*)}, \dots, \boldsymbol{\beta}^{(N_{\Delta_t}-1)}\right)^\top \\
&\quad \text{with} \quad \boldsymbol{\beta}^{(\ell)} = \left(\boldsymbol{\beta}_1^{(\ell)}, \boldsymbol{\beta}_2^{(\ell)}, \dots, \boldsymbol{\beta}_{M_{\Delta_\mathrm{x}}}^{(\ell)}\right)^\top .
\end{aligned}
\tag{4.12}
$$

The solution of (4.11) is obtained by a block forward substitution, i.e. at every time instant t_ℓ, with $\ell = 0, \dots, N_{\Delta_t} - 1$, one computes

$$
\begin{aligned}
\mathbf{z}^{(\ell)} &= \boldsymbol{\beta}^{(\ell)} - \sum_{j=1}^{\ell^*} \mathbb{E}^{(j)} \boldsymbol{\alpha}^{(\ell-j)} \\
&\quad \text{with} \quad \ell^* := \min\{\ell, N^* - 1\},
\end{aligned}
\tag{4.13}
$$

and then solves the reduced linear system

$$
\mathbb{E}^{(0)} \boldsymbol{\alpha}^{(\ell)} = \mathbf{z}^{(\ell)}. \tag{4.14}
$$

Procedure (4.13) and (4.14) is a time-marching technique, where the only matrix to be inverted is the non-singular block $\mathbb{E}^{(0)}$; therefore the LU factorization needs to be performed only once and stored. Then, at each time step, the solution of (4.14) requires only a forward and a backward substitution phases. All the other blocks $\mathbb{E}^{(\ell)}$, with $\ell = 1, \dots, N^* - 1$, are used to update at every time step the right-hand side. Of course, due to the whole matrix $\mathbb{E}$ structure, one can construct and store only blocks $\mathbb{E}^{(0)}, \dots, \mathbb{E}^{(N^*-1)}$ with a considerable reduction in the computational cost and the memory requirement.

Remark We stress that the crucial point for the success of the energetic BEM is the careful numerical evaluation of the entries of the block $\mathbb{E}^{(0)}$ that must take place under the assumption that all the involved integrals are computed with a sufficiently high accuracy.

Remark The proposed energetic weak formulation, after time integration, can be regarded as a Newmark scheme with parameters $\zeta = 1/2$ and $\theta = 1$ in the notation of [33], as proved for scalar problems in [6, 7] in the more general framework of Energetic BEM-FEM coupling. This particular Newmark scheme is implicit, unconditionally stable and first-order accurate in Δt. Furthermore, the theoretical analysis about convergence and space–time accuracy in the context of 3D elastodynamic problems has been performed in [10].

5 Quadrature of double integrals in space variables

In this section we focus on the efficient computation of the space integrals appearing in (4.7), which is essential for the numerical stability of the EBEM. Since we use piecewise constant basis and test functions, we can reduce the integrals over Γ to double integrals over the source and the field triangles $E_{\tilde{m}}$ and E_m respectively:

$$
\begin{aligned}
\mathbb{E}^{(\ell)}_{\tilde{m},m} &= -\frac{1}{4\pi\varrho} \sum_{\eta,\tilde{\eta}=0}^{1} (-1)^{\eta+\tilde{\eta}} \\
&\qquad \int_{E_{\tilde{m}}} \int_{E_m} \mathbb{G}(\mathbf{x}, \mathbf{y}; \Delta_{\tilde{n}+\tilde{\eta}, n+\eta}) d\Gamma_{\mathbf{y}} d\Gamma_{\mathbf{x}}.
\end{aligned}
\tag{5.1}
$$

The outer integration on the source triangle is carried out by applying a M_g-point suitable quadrature rule, so that

$$
\begin{aligned}
\mathbb{E}^{(\ell)}_{\tilde{m},m} &\simeq -\frac{1}{4\pi\varrho} \sum_{\eta,\tilde{\eta}=0}^{1} (-1)^{\eta+\tilde{\eta}} \sum_{q=1}^{M_g} \omega_q \\
&\qquad \int_{E_m} \mathbb{G}(\mathbf{x}_q, \mathbf{y}; \Delta_{\tilde{n}+\tilde{\eta}, n+\eta}) d\Gamma_{\mathbf{y}},
\end{aligned}
\tag{5.2}
$$

where $\mathbf{x}_q$ and ω_q are the quadrature nodes and weights, respectively. The same strategy can in principle be used for

Journal: 466 MS: 2312 TYPESET DISK LE CP Disp.:2023/3/30 Pages: 21 Layout: Large

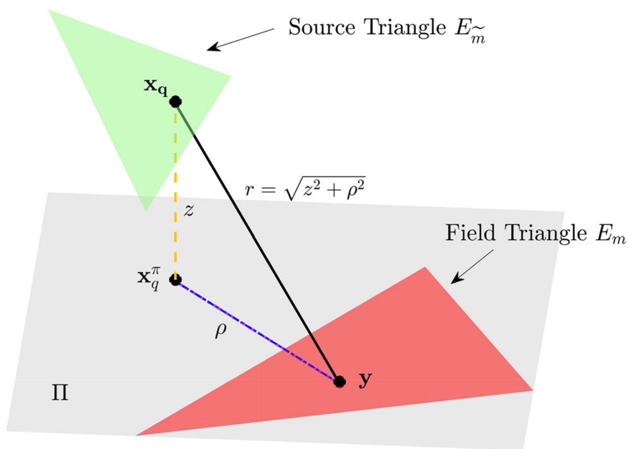

Fig. 1 Projection of the source point $\mathbf{x}_q$ onto the plane of the inner (field) triangle of integration

the numerical computation of the integral over the field triangle but standard quadrature formulas would require a very large number of quadrature nodes, due to the low regularity of the time integrated kernel. Furthermore, it is worth noting that, in this case, the implementation is complicated since the integration domain is defined by the intersection of the field triangle and the wavefronts of the P- and S-waves. In particular, the presence of the Heaviside functions in (4.8) implies that the integration over E_m has to be in general limited to the portion enclosed between two spherical surfaces of radii $r_\text{P} = c_\text{P}\Delta_{\tilde{n},n}$ and $r_\text{S} = c_\text{S}\Delta_{\tilde{n},n}$ respectively, both centered at $\mathbf{x}_q$. In order to avoid excessive simplifications in dealing with such integration domains, that may strongly affect the stability properties of the EBEM, we follow the strategy suggested in [29] for the scalar wave equation. First of all, we project the source point $\mathbf{x}_q$ into the plane Π containing the triangle E_m and we call $\mathbf{x}_q^\pi$ the projection point, as depicted in Fig. 1.

Then, we apply a coordinate transformation maintaining the distances and mapping the point $\mathbf{x}_q^\pi$ into the origin $\hat{\mathbf{O}} = (0, 0, 0)$ and the canonical system $\mathbf{e}_1, \mathbf{e}_2, \mathbf{e}_3$ of the Euclidean space $\mathbf{R}^3$ into the triplet $\hat{\mathbf{e}}_1, \hat{\mathbf{e}}_2, \hat{\mathbf{e}}_3$ where $\hat{\mathbf{e}}_3$ is the direction perpendicular to the plane Π while $\hat{\mathbf{e}}_1$ is parallel to a chosen side of the field triangle E_m. As a consequence, we have that the new coordinates of $\mathbf{x}_q$ are $\hat{\mathbf{x}}_q = (0, 0, z)$, where $z := |\mathbf{x}_q - \mathbf{x}_q^\pi|$. This transformation is a translation and a rotation, so that the arbitrary point $\mathbf{y} = (y_1, y_2, y_3)$ is mapped into the point $\hat{\mathbf{y}} = (\hat{y}_1, \hat{y}_2, \hat{y}_3)$ related to it through the relations:

$$\mathbf{y} = \mathbf{x}_q^\pi + \mathbb{S}\hat{\mathbf{y}} \quad \text{and} \quad \hat{\mathbf{y}} = \mathbb{S}^{-1}(\mathbf{y} - \mathbf{x}_q^\pi), \tag{5.3}$$

where $\mathbb{S}$ is the orthogonal rotation matrix with $|\det(\mathbb{S})| = 1$. Considering the change of variable in (5.3), we derive the relation between the kernel $\mathbb{G}$ with respect to the old coordinates system and the corresponding kernel $\hat{\mathbb{G}}$ with respect to the new coordinates system, i.e. $\mathbb{G} = \mathbb{S}^{-1}\hat{\mathbb{G}}\mathbb{S}$. As the consequence, we obtain:

$$\mathbb{E}^{(\ell)}_{\tilde{m},m} \simeq -\frac{1}{4\pi\varrho}\sum_{\eta,\tilde{\eta}=0}^{1}(-1)^{\eta+\tilde{\eta}}\sum_{q=1}^{\nu}\omega_q \int_{\hat{E}_m}\mathbb{S}^{-1}\hat{\mathbb{G}}(\hat{\mathbf{x}}_q,\hat{\mathbf{y}};\,\Delta_{\tilde{n}+\tilde{\eta},n+\eta})\mathbb{S}\,\mathrm{d}\Gamma_{\hat{\mathbf{y}}}. \tag{5.4}$$

At this stage, we express the inner integration over the field triangle $\hat{E}_m$ (father) as an algebraic sum of integrals over three triangles $\hat{E}_m^{(k)}$ (children), $k = 1, 2, 3$, having $\hat{\mathbf{O}}$, $\hat{\mathbf{y}}_1^{(k)}$ and $\hat{\mathbf{y}}_2^{(k)}$ as vertices (see Fig. 2). Consequently, we have:

$$\mathbb{E}^{(\ell)}_{\tilde{m},m} \simeq -\frac{1}{4\pi\varrho}\sum_{\eta,\tilde{\eta}=0}^{1}(-1)^{\eta+\tilde{\eta}}\sum_{q=1}^{\nu}\omega_q\sum_{k=1}^{3}\varsigma_k \int_{\hat{E}_m^{(k)}}\mathbb{S}^{-1}\hat{\mathbb{G}}(\hat{\mathbf{x}}_q,\hat{\mathbf{y}};\,\Delta_{\tilde{n}+\tilde{\eta},n+\eta})\mathbb{S}\,\mathrm{d}\Gamma_{\hat{\mathbf{y}}}, \tag{5.5}$$

where the coefficients ς_k are given by

$$\varsigma_k := \operatorname{sign}\left(\begin{vmatrix} 1 & 0 & 0 \\ 1 & \hat{y}_{1,1}^{(k)} & \hat{y}_{1,2}^{(k)} \\ 1 & \hat{y}_{2,1}^{(k)} & \hat{y}_{2,2}^{(k)} \end{vmatrix}\right) = \begin{cases} -1, & \text{if } \hat{y}_{1,1}^{(k)}\hat{y}_{2,2}^{(k)} - \hat{y}_{1,2}^{(k)}\hat{y}_{2,1}^{(k)} < 0 \\ 0, & \text{if } \hat{y}_{1,1}^{(k)}\hat{y}_{2,2}^{(k)} - \hat{y}_{1,2}^{(k)}\hat{y}_{2,1}^{(k)} = 0 \\ 1, & \text{if } \hat{y}_{1,1}^{(k)}\hat{y}_{2,2}^{(k)} - \hat{y}_{1,2}^{(k)}\hat{y}_{2,1}^{(k)} > 0. \end{cases}$$

Each of the children triangles is now addressed separately. For a given $\hat{E}_m^{(k)}$, the lengths of its sides are defined to be:

$$a := |\hat{\mathbf{y}}_1^{(k)} - \hat{\mathbf{O}}|, \qquad b := |\hat{\mathbf{y}}_2^{(k)} - \hat{\mathbf{O}}| \quad \text{and} \quad c := |\hat{\mathbf{y}}_2^{(k)} - \hat{\mathbf{y}}_1^{(k)}|,$$

while its angles are defined via Carnot's theorem as

$$\alpha = \operatorname{acos}\left(\frac{b^2+c^2-a^2}{2bc}\right), \quad \beta = \operatorname{acos}\left(\frac{a^2+c^2-b^2}{2ac}\right) \quad \text{and} \quad \gamma = \operatorname{acos}\left(\frac{a^2+b^2-c^2}{2ab}\right)$$

with $0 \le \alpha, \beta, \gamma \le \pi$ and $\alpha + \beta + \gamma = \pi$.
We make a counterclockwise rotation in the plane Π by an angle δ about the $\hat{\mathbf{e}}_3$-axis, so that we introduce a new coordinate frame consisting of the origin $\check{\mathbf{O}} = \hat{\mathbf{O}}$ and mutually orthogonal axes in the directions of the unit vectors $\check{\mathbf{e}}_1, \check{\mathbf{e}}_2$ and $\check{\mathbf{e}}_3 = \hat{\mathbf{e}}_3$. This change of variable, which maps the point $\hat{\mathbf{y}}_1^{(k)}$

Journal: 466 MS: 2312 TYPESET DISK LE CP Disp.:2023/3/30 Pages: 21 Layout: Large

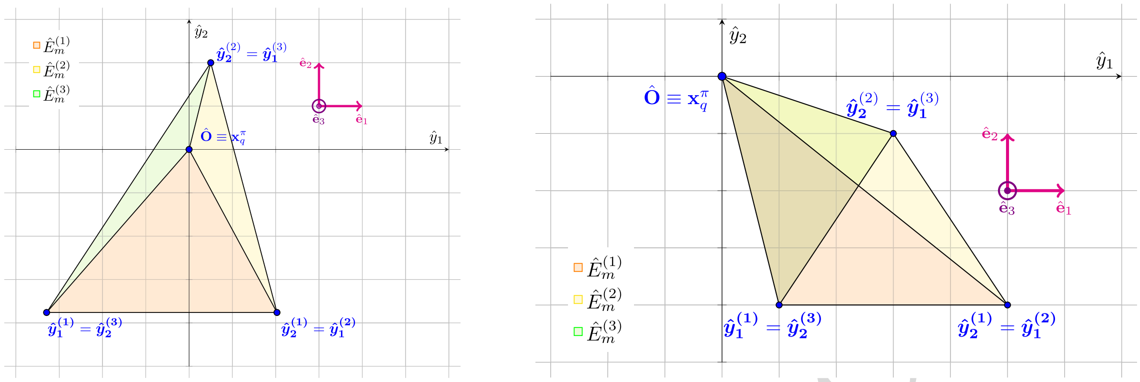

Fig. 2 Decomposition of the field triangle $\hat{E}_m$ (father) into three triangles $\hat{E}_m^{(k)}$ (children), $k = 1, 2, 3$, having $\hat{\mathbf{O}}$, $\hat{\mathbf{y}}_1^{(k)}$ and $\hat{\mathbf{y}}_2^{(k)}$ as vertices. On the left plot, the point $\hat{\mathbf{O}} \equiv \hat{\mathbf{x}}_q$ is inside the triangle $\hat{E}_m$. On the right plot, the point $\hat{\mathbf{O}} \equiv \hat{\mathbf{x}}_q$ is outside the triangle $\hat{E}_m$

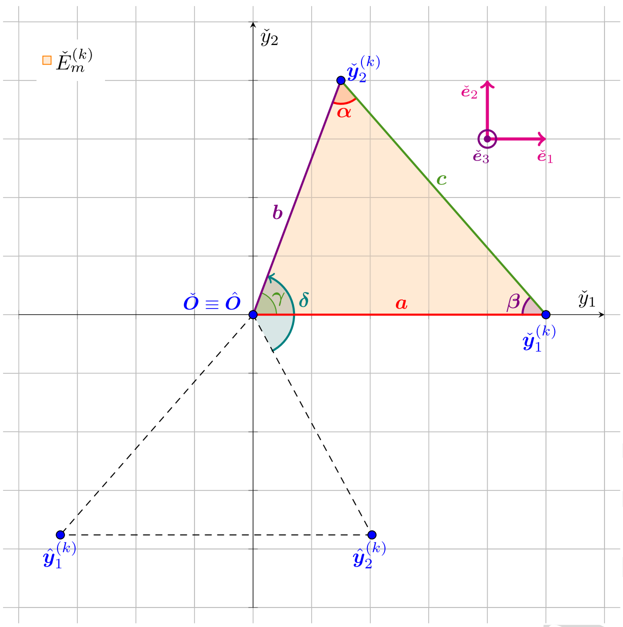

Fig. 3 Counterclockwise rotation in the plane Π by an angle δ about the $\hat{\mathbf{e}}_3$-axis. The new coordinate frame has the origin at $\check{\mathbf{O}} = \hat{\mathbf{O}}$ and mutually orthogonal axes in the directions of the unit vectors $\check{\mathbf{e}}_1$, $\check{\mathbf{e}}_2$ and $\check{\mathbf{e}}_3 = \hat{\mathbf{e}}_3$

into the point $\check{\mathbf{y}}_1^{(k)} = (a, 0, 0)$, is represented by the matrix equations:

$$\hat{\mathbf{y}} = \mathbb{T}\check{\mathbf{y}} \quad \text{and} \quad \check{\mathbf{y}} = \mathbb{T}^{-1}\hat{\mathbf{y}}, \quad \text{with} \quad |\det(\mathbb{T})| = 1 \tag{5.6}$$

as depicted in Fig. 3.

Therefore, Eq. (5.5) is recast in the following form

$$\mathbb{E}_{\tilde{m},m}^{(\ell)} \simeq -\frac{1}{4\pi\varrho} \sum_{\eta,\tilde{\eta}=0}^{1} (-1)^{\eta+\tilde{\eta}} \sum_{q=1}^{\nu} \omega_q \sum_{k=1}^{3} \varsigma_k \int_{\check{E}_m^{(k)}} \mathbb{S}^{-1}\mathbb{T}^{-1}\check{\mathbb{G}}(\check{\mathbf{x}}_q, \check{\mathbf{y}}; \Delta_{\tilde{n}+\tilde{\eta},n+\eta})\mathbb{T}\mathbb{S}\mathrm{d}\Gamma_{\check{\mathbf{y}}}. \tag{5.7}$$

We point out that the benefits of the above described apparently cumbersome procedure are extremely significant. In fact, it is worth noting that it allows for the exact detection of the integration domain and, consequently, for the analytical computation of the integrals in (5.7), as we will explain in the following subsections.

5.1 Exact representation of the wave fronts

As z is constant for the integral over $\check{E}_m^{(k)}$, we fix the plane $\check{\mathbf{e}}_1$-$\check{\mathbf{e}}_2$ as a working plane and we select an intrinsic 2D polar coordinate system (ρ, θ) with origin at $\check{\mathbf{O}} := (0, 0)$, so that the distance $\check{r} = |\check{\mathbf{x}}_q - \check{\mathbf{y}}|$ becomes $\check{r} = \sqrt{z^2 + \rho^2}$, while the components of the distance vector $\check{\mathbf{r}} = \check{\mathbf{x}}_q - \check{\mathbf{y}}$ are given by:

$$\check{r}_i = \frac{\rho}{\sin\gamma}\left[A_{1i}\sin(\gamma - \theta) + A_{2i}\sin(\theta)\right] + A_{3i}z, \quad i = 1, 2, 3, \tag{5.8}$$

where the coefficients A_{1i}, A_{2i} and A_{3i} are defined as follows:

$$A_{1i} := \frac{1}{a}\check{\mathbf{y}}_1^{(k)} \cdot \check{\mathbf{e}}_i, \quad A_{2i} := \frac{1}{b}\check{\mathbf{y}}_2^{(k)} \cdot \check{\mathbf{e}}_i$$

$$\text{and} \quad A_{3i} := \frac{1}{z}\left(\check{\mathbf{x}}_q - \check{\mathbf{O}}\right) \cdot \check{\mathbf{e}}_i.$$

As a consequence of relation (5.8), for each $i,\ j = 1, 2, 3$ we have

$$\begin{aligned}\check{r}_i\check{r}_j = \frac{\rho^2}{\sin^2\gamma}\Big[&A_{1i}A_{1j}\sin^2(\gamma-\theta) + (A_{1i}A_{2j} + A_{2i}A_{1j})\\ &\sin(\gamma-\theta)\sin(\theta) + A_{2i}A_{2j}\sin^2\theta\Big]\\ &+ z\frac{\rho}{\sin\gamma}\Big[(A_{1i}A_{3j} + A_{3i}A_{1j})\sin(\gamma-\theta)\\ &+ (A_{2i}A_{3j} + A_{3i}A_{2j})\sin\theta\Big] + z^2A_{3i}A_{3j}.\end{aligned} \tag{5.9}$$

Furthermore, the distance $R(\theta)$ between a point $\check{\mathbf{y}}$ on the side $\check{\mathbf{y}}_2^{(k)} - \check{\mathbf{y}}_1^{(k)}$ and the origin $\check{\mathbf{O}}$ is of particular importance for integration purposes and it is given by

$$R(\theta) := \frac{F}{\sin(\theta+\beta)}$$
$$\text{with}\quad F = a\sin\beta \quad\text{and}\quad \theta \in (-\beta, \pi-\beta).$$

In order to establish a simple and general procedure to account for the presence of the wavefronts in an exact way, we remark that in the working plane they are represented by two circles of radii $\rho_{\mathrm{P}} = \sqrt{r_{\mathrm{P}}^2 - z^2}$ and $\rho_{\mathrm{S}} = \sqrt{r_{\mathrm{S}}^2 - z^2}$, both centred at $\check{\mathbf{O}}$. Moreover, when $r_{\mathrm{S}} < z < r_{\mathrm{P}}$, only the P-wave front intersects the plane Π, inducing the partition of $\check{E}_m^{(k)}$ depicted in the left plot of Fig. 4 and represented by (the sum of) the three possible sub-regions:

$$\mathcal{R}_1 := \left\{(\rho,\theta) \mid \theta \in \left[0, \min\{\max\{0,\theta_1\},\gamma\}\right],\ \rho \in [0,\rho_{\mathrm{P}}]\right\}$$
$$\mathcal{R}_2 := \left\{(\rho,\theta) \mid \theta \in \left[\min\{\max\{0,\theta_1\},\gamma\}, \max\{0,\min\{\theta_2,\gamma\}\}\right],\ \rho \in [0, R(\theta)]\right\}$$
$$\mathcal{R}_3 := \left\{(\rho,\theta) \mid \theta \in \left[\max\{0,\min\{\theta_2,\gamma\}\},\gamma\right],\ \rho \in [0,\rho_{\mathrm{P}}]\right\}$$

where the angles θ_1 and θ_2 are the slopes of the rays joining the origin $\check{\mathbf{O}}$ with all the intersections between the P-wave front and the whole extension line of the side $\check{\mathbf{y}}_2^{(k)} - \check{\mathbf{y}}_1^{(k)}$ of the triangle $\check{E}_m^{(k)}$. Note that these intersections may lie outside the triangle.

Otherwise, i.e. when $z < r_{\mathrm{S}} < r_{\mathrm{P}}$, both the P- and the S-wave fronts are active. As a consequence, this scenario is more complicated than the previous one, because the integration domain (as illustrated in the right plot of Fig. 4) is made by the seven possible sub-regions

$$\mathcal{Q}_1 := \left\{(\rho,\theta) \mid \theta \in \left[0, \min\{\max\{0,\theta_1\},\gamma\}\right],\ \rho \in [0,\rho_{\mathrm{S}}]\right\}$$
$$\mathcal{Q}_2 := \left\{(\rho,\theta) \mid \theta \in \left[\min\{\max\{0,\theta_1\},\gamma\}, \max\{0,\min\{\theta_2,\gamma\}\}\right],\ \rho \in [0, R(\theta)]\right\}$$
$$\mathcal{Q}_3 := \left\{(\rho,\theta) \mid \theta \in \left[\max\{0,\min\{\theta_2,\gamma\}\},\gamma\right],\ \rho \in [0,\rho_{\mathrm{S}}]\right\}$$
$$\mathcal{Q}_4 := \left\{(\rho,\theta) \mid \theta \in \left[0, \min\{\max\{0,\theta_3\},\gamma\}\right],\ \rho \in [\rho_{\mathrm{S}},\rho_{\mathrm{P}}]\right\}$$
$$\mathcal{Q}_5 := \left\{(\rho,\theta) \mid \theta \in \left[\min\{\max\{0,\theta_3\},\gamma\}, \min\{\max\{0,\theta_1\},\gamma\}\right],\ \rho \in [\rho_{\mathrm{S}}, R(\theta)]\right\}$$
$$\mathcal{Q}_6 := \left\{(\rho,\theta) \mid \theta \in \left[\max\{0,\min\{\theta_2,\gamma\}\}, \max\{0,\min\{\theta_4,\gamma\}\}\right],\ \rho \in [\rho_{\mathrm{S}}, R(\theta)]\right\}$$
$$\mathcal{Q}_7 := \left\{(\rho,\theta) \mid \theta \in \left[\max\{0,\min\{\theta_4,\gamma\}\},\gamma\right],\ \rho \in [\rho_{\mathrm{S}},\rho_{\mathrm{P}}]\right\}$$

where the angles θ_1, θ_2, θ_3 and θ_4 are the slopes of the rays joining the origin $\check{\mathbf{O}}$ with all the intersections between the P- and S-wave fronts and the whole extension line of the side $\check{\mathbf{y}}_2^{(k)} - \check{\mathbf{y}}_1^{(k)}$ of the triangle $\check{E}_m^{(k)}$.

Looking at Fig. 4, we remark that the sub-regions may be traced back to four different shapes. For this reason, in order to describe the analytical procedure to compute the integrals in (5.7), we refer to the four reference integration domains illustrated in Fig. 5, i.e.

$$\mathcal{E} := \left\{(\rho,\theta) \mid \theta_{\diamondsuit} \le \theta \le \theta_{\heartsuit} \text{ and } 0 \le \rho \le \rho_{\spadesuit}\right\}$$
$$\mathcal{F} := \left\{(\rho,\theta) \mid \theta_{\diamondsuit} \le \theta \le \theta_{\heartsuit} \text{ and } \rho_{\clubsuit} \le \rho \le \rho_{\spadesuit}\right\}$$
$$\mathcal{G} := \left\{(\rho,\theta) \mid \theta_{\diamondsuit} \le \theta \le \theta_{\heartsuit} \text{ and } 0 \le \rho \le R(\theta)\right\}$$
$$\mathcal{H} := \left\{(\rho,\theta) \mid \theta_{\diamondsuit} \le \theta \le \theta_{\heartsuit} \text{ and } \rho_{\clubsuit} \le \rho \le R(\theta)\right\}.$$

We point out that, when $\rho_{\clubsuit} = 0$, the regions $\mathcal{F}$ and $\mathcal{H}$ collapse into $\mathcal{E}$ and $\mathcal{G}$, respectively. For this reason, we are going to detail the analytical integration only over the former domains, i.e. we are going to consider

$$I_1^{\mathcal{D}} := \int_{\mathcal{D}} \frac{1}{\check{r}}\mathrm{d}\Gamma_{\check{\mathbf{y}}}, \quad I_2^{\mathcal{D}} := \int_{\mathcal{D}} \frac{\check{r}_i\check{r}_j}{\check{r}^3}\mathrm{d}\Gamma_{\check{\mathbf{y}}},$$
$$I_3^{\mathcal{D}} := \int_{\mathcal{D}} \frac{\check{r}_i\check{r}_j}{\check{r}^5}\mathrm{d}\Gamma_{\check{\mathbf{y}}} \quad\text{and}\quad I_4^{\mathcal{D}} := \int_{\mathcal{D}} \frac{1}{\check{r}^3}\mathrm{d}\Gamma_{\check{\mathbf{y}}}, \tag{5.10}$$

with $\mathcal{D} = \mathcal{F}, \mathcal{H}$. Since both the integration domains are described in terms of polar coordinates, we convert the above integrals, taking into account (5.9) and remembering that the elemental area $\mathrm{d}\Gamma_{\check{\mathbf{y}}}$ changes according to the formula $\mathrm{d}\Gamma_{\check{\mathbf{y}}} = \rho\mathrm{d}\rho\mathrm{d}\theta$. We point out that the results presented in the following two sub-sections extend those in [31].

5.2 Integrals over the region $\mathcal{F}$

When $\mathcal{D} = \mathcal{F}$, plugging the polar coordinates into the double integrals in (5.10) gives rise to separable integrals of the type:

$$\int_{\theta_{\diamondsuit}}^{\theta_{\heartsuit}} (\sin\theta)^{k-1}(\sin(\gamma-\theta))^{h-1}\,\mathrm{d}\vartheta \int_{\rho_{\clubsuit}}^{\rho_{\spadesuit}} \frac{\varrho^i}{\left(\varrho^2+z^2\right)^{j/2}}\mathrm{d}\varrho$$
$$:= \Theta_{k,h}(\theta_{\diamondsuit},\theta_{\heartsuit})K_{i,j}(\rho_{\clubsuit},\rho_{\spadesuit}),$$

where the indices $h, k = 1, 2, 3$ are such that $2 \le h+k < 5$, while the indices i and j are such that $i = j = 1$ or $i = 1, 2, 3$

Journal: 466 MS: 2312 TYPESET DISK LE CP Disp.:2023/3/30 Pages: 21 Layout: Large

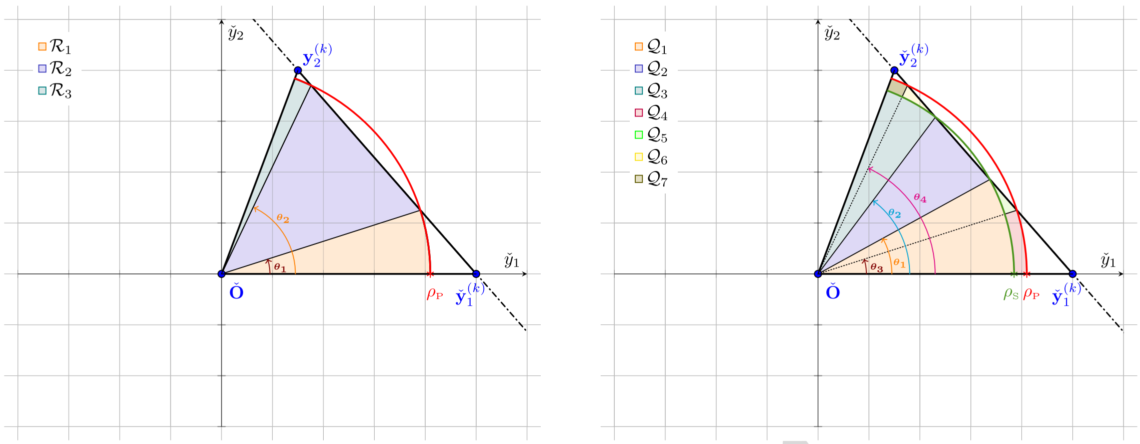

Fig. 4 General partition of one triangle $\check{E}_m^{(k)}$ due to the wave fronts. On the left plot, only the P-wave front is active. On the right plot, both the P-wave and S-wave fronts are active

Fig. 5 The four reference integration domains

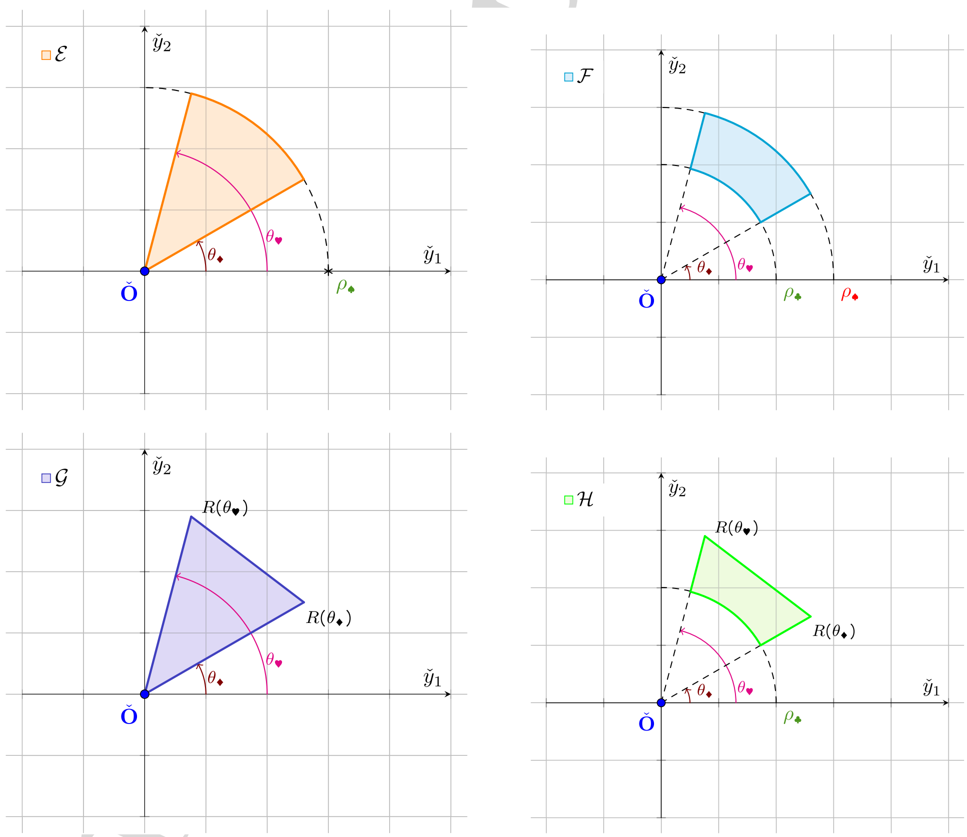

and $j = 3, 5$. It easy to check that the integration in variable ϱ produces the functions:

$$K_{1,1}(\rho_\clubsuit, \rho_\spadesuit) := \sqrt{\rho_\spadesuit^2 + z^2} - \sqrt{\rho_\clubsuit^2 + z^2}$$

$$K_{1,3}(\rho_\clubsuit, \rho_\spadesuit) := -\frac{1}{\sqrt{\rho_\spadesuit^2 + z^2}} + \frac{1}{\sqrt{\rho_\clubsuit^2 + z^2}}$$

$$K_{1,5}(\rho_\clubsuit, \rho_\spadesuit) := \frac{1}{3}\left[\left(\frac{1}{\sqrt{\rho_\clubsuit^2 + z^2}}\right)^3 - \left(\frac{1}{\sqrt{\rho_\spadesuit^2 + z^2}}\right)^3\right]$$

$$K_{2,3}(\rho_\clubsuit, \rho_\spadesuit)$$

$$:= \log\left(\frac{\rho_\spadesuit + \sqrt{\rho_\spadesuit^2 + z^2}}{\rho_\clubsuit + \sqrt{\rho_\clubsuit^2 + z^2}}\right) - \frac{\rho_\spadesuit}{\sqrt{\rho_\spadesuit^2 + z^2}} + \frac{\rho_\clubsuit}{\sqrt{\rho_\clubsuit^2 + z^2}}$$

$$K_{2,5}(\rho_\clubsuit, \rho_\spadesuit) := \frac{1}{3z^2}$$

Journal: **466** MS: **2312** ☐ TYPESET ☐ DISK ☐ LE ☐ CP Disp.:**2023/3/30** Pages: **21** Layout: **Large**

$$\left[\left(\frac{\rho_{\spadesuit}}{\sqrt{\rho_{\spadesuit}^2+z^2}}\right)^3-\left(\frac{\rho_{\clubsuit}}{\sqrt{\rho_{\clubsuit}^2+z^2}}\right)^3\right]$$

$$K_{3,3}(\rho_{\clubsuit},\rho_{\spadesuit}) := \sqrt{\rho_{\spadesuit}^2+z^2}-\sqrt{\rho_{\clubsuit}^2+z^2}+z^2$$
$$\left(\frac{1}{\sqrt{\rho_{\spadesuit}^2+z^2}}-\frac{1}{\sqrt{\rho_{\clubsuit}^2+z^2}}\right)$$

$$K_{3,5}(\rho_{\clubsuit},\rho_{\spadesuit}) := \frac{1}{\sqrt{\rho_{\clubsuit}^2+z^2}}-\frac{1}{\sqrt{\rho_{\spadesuit}^2+z^2}}+\frac{z^2}{3}$$
$$\left[\left(\frac{1}{\sqrt{\rho_{\spadesuit}^2+z^2}}\right)^3-\left(\frac{1}{\sqrt{\rho_{\clubsuit}^2+z^2}}\right)^3\right]$$

while the results of the integration in variable θ are:

$$\Theta_{1,1}(\theta_{\vardiamondsuit},\theta_{\varheartsuit}) := \theta_{\varheartsuit}-\theta_{\vardiamondsuit}$$
$$\Theta_{1,2}(\theta_{\vardiamondsuit},\theta_{\varheartsuit}) := 2\sin\left(\frac{\theta_{\varheartsuit}-\theta_{\vardiamondsuit}}{2}\right)\sin\left(\gamma-\frac{\theta_{\varheartsuit}+\theta_{\vardiamondsuit}}{2}\right)$$
$$\Theta_{1,3}(\theta_{\vardiamondsuit},\theta_{\varheartsuit})$$
$$:= \frac{1}{2}\left[\theta_{\varheartsuit}-\theta_{\vardiamondsuit}-\sin(\theta_{\varheartsuit}-\theta_{\vardiamondsuit})\cos(2\gamma-\theta_{\varheartsuit}-\theta_{\vardiamondsuit})\right]$$
$$\Theta_{2,1}(\theta_{\vardiamondsuit},\theta_{\varheartsuit}) := 2\sin\left(\frac{\theta_{\varheartsuit}-\theta_{\vardiamondsuit}}{2}\right)\sin\left(\frac{\theta_{\varheartsuit}+\theta_{\vardiamondsuit}}{2}\right)$$
$$\Theta_{2,2}(\theta_{\vardiamondsuit},\theta_{\varheartsuit})$$
$$:= \frac{1}{2}\left[\sin(\theta_{\varheartsuit}-\theta_{\vardiamondsuit})\cos(\gamma-\theta_{\varheartsuit}-\theta_{\vardiamondsuit})-(\theta_{\varheartsuit}-\theta_{\vardiamondsuit})\cos\gamma\right]$$
$$\Theta_{3,1}(\theta_{\vardiamondsuit},\theta_{\varheartsuit})$$
$$:= \frac{1}{2}\left[\theta_{\varheartsuit}-\theta_{\vardiamondsuit}-\sin(\theta_{\varheartsuit}-\theta_{\vardiamondsuit})\cos(\theta_{\varheartsuit}+\theta_{\vardiamondsuit})\right].$$

Due to the above computations, when $z>0$ we can conclude that

$$I_1^{\mathcal{F}} = \Theta_{1,1}(\theta_{\vardiamondsuit},\theta_{\varheartsuit})K_{1,1}(\rho_{\clubsuit},\rho_{\spadesuit}) \quad \text{and}$$
$$I_4^{\mathcal{F}} = \Theta_{1,1}(\theta_{\vardiamondsuit},\theta_{\varheartsuit})K_{1,3}(\rho_{\clubsuit},\rho_{\spadesuit})$$

while

$$I_2^{\mathcal{F}} = \frac{K_{3,3}(\rho_{\clubsuit},\rho_{\spadesuit})}{\sin^2\gamma}\left[A_{1i}A_{1j}\Theta_{1,3}(\theta_{\vardiamondsuit},\theta_{\varheartsuit})\right.$$
$$+(A_{1i}A_{2j}+A_{2i}A_{1j})\Theta_{2,2}(\theta_{\vardiamondsuit},\theta_{\varheartsuit})$$
$$\left.+A_{2i}A_{2j}\Theta_{3,1}(\theta_{\vardiamondsuit},\theta_{\varheartsuit})\right]+z\frac{K_{2,3}(\rho_{\clubsuit},\rho_{\spadesuit})}{\sin\gamma}$$
$$\left[(A_{1i}A_{3j}+A_{3i}A_{1j})\Theta_{1,2}(\theta_{\vardiamondsuit},\theta_{\varheartsuit})\right.$$
$$\left.+(A_{2i}A_{3j}+A_{3i}A_{2j})\Theta_{2,1}(\theta_{\vardiamondsuit},\theta_{\varheartsuit})\right]$$
$$+z^2K_{1,3}(\rho_{\clubsuit},\rho_{\spadesuit})\Theta_{1,1}(\theta_{\vardiamondsuit},\theta_{\varheartsuit})A_{3i}A_{3j}$$

and

$$I_3^{\mathcal{F}} = \frac{K_{3,5}(\rho_{\clubsuit},\rho_{\spadesuit})}{\sin^2\gamma}$$
$$\left[A_{1i}A_{1j}\Theta_{1,3}(\theta_{\vardiamondsuit},\theta_{\varheartsuit})+(A_{1i}A_{2j}+A_{2i}A_{1j})\Theta_{2,2}\right.$$
$$\left.(\theta_{\vardiamondsuit},\theta_{\varheartsuit})+A_{2i}A_{2j}\Theta_{3,1}(\theta_{\vardiamondsuit},\theta_{\varheartsuit})\right]$$
$$+z\frac{K_{2,5}(\rho_{\clubsuit},\rho_{\spadesuit})}{\sin\gamma}$$
$$\left[(A_{1i}A_{3j}+A_{3i}A_{1j})\Theta_{1,2}(\theta_{\vardiamondsuit},\theta_{\varheartsuit})\right.$$
$$\left.+(A_{2i}A_{3j}+A_{3i}A_{2j})\Theta_{2,1}(\theta_{\vardiamondsuit},\theta_{\varheartsuit})\right]$$
$$+z^2K_{1,5}(\rho_{\clubsuit},\rho_{\spadesuit})\Theta_{1,1}(\theta_{\vardiamondsuit},\theta_{\varheartsuit})A_{3i}A_{3j}.$$

Remark In Appendix A we report the values of $K_{i,j}(0,\rho_{\spadesuit})$ for $i=j=1$ or $i=1,2,3$ and $j=3,5$. These quantities are useful to compute the integrals over the integration domain $\mathcal{E}$.
Remark When the field and the source triangles lay on the same plane, i.e. $z=0$, with the help of a limit process that makes z tending to 0, it is easy to show that

$$I_1^{\mathcal{F}} = \Theta_{1,1}(\theta_{\vardiamondsuit},\theta_{\varheartsuit})K_1^* \quad \text{and} \quad I_4^{\mathcal{F}} = \Theta_{1,1}(\theta_{\vardiamondsuit},\theta_{\varheartsuit})K_2^*$$

while

$$I_2^{\mathcal{F}} = \frac{K_1^*}{\sin^2\gamma}\left[A_{1i}A_{1j}\Theta_{1,3}(\theta_{\vardiamondsuit},\theta_{\varheartsuit})+(A_{1i}A_{2j}\right.$$
$$\left.+A_{2i}A_{1j})\Theta_{2,2}(\theta_{\vardiamondsuit},\theta_{\varheartsuit})+A_{2i}A_{2j}\Theta_{3,1}(\theta_{\vardiamondsuit},\theta_{\varheartsuit})\right]$$
$$I_3^{\mathcal{F}} = \frac{K_2^*}{\sin^2\gamma}\left[A_{1i}A_{1j}\Theta_{1,3}(\theta_{\vardiamondsuit},\theta_{\varheartsuit})\right.$$
$$\left.+(A_{1i}A_{2j}+A_{2i}A_{1j})\Theta_{2,2}(\theta_{\vardiamondsuit},\theta_{\varheartsuit})+A_{2i}A_{2j}\Theta_{3,1}(\theta_{\vardiamondsuit},\theta_{\varheartsuit})\right],$$

where the constants K_1^* and K_2^* following values:

$$K_1^* := (c_P-c_S)\Delta_{n,\tilde{n}} \quad \text{and} \quad K_2^* := \frac{1}{\Delta_{n,\tilde{n}}}\frac{c_P-c_S}{c_Pc_S}.$$

5.3 Integrals over the region $\mathcal{H}$

If we consider the domain $\mathcal{D}=\mathcal{H}$ in (5.10) and we use polar coordinates, we obtain double integrals of the type:

$$\int_{\theta_{\vardiamondsuit}}^{\theta_{\varheartsuit}}(\sin\theta)^{k-1}(\sin(\gamma-\theta))^{h-1}K_{i,j}(\rho_{\clubsuit},R(\theta))\mathrm{d}\vartheta$$
$$:= \widetilde{K}_{i,j}^{k,h}(\rho_{\clubsuit};\theta_{\vardiamondsuit},\theta_{\varheartsuit}),$$

where the indices $h,k=1,2,3$ are such that $2\le h+k<5$, while the indices i and j are such that $i=j=1$ or $i=1,2,3$ and $j=3,5$. The computation of $\widetilde{K}_{i,j}^{k,h}(\rho_{\clubsuit};\theta_{\vardiamondsuit},\theta_{\varheartsuit})$ is not

Journal: 466 MS: 2312 TYPESET DISK LE CP Disp.:2023/3/30 Pages: 21 Layout: Large

straightforward, since it requires the knowledge of sophisticated relationships linking the complex logarithm to the inverse or hyperbolic sine and cosine, collected in [1]. Furthermore, the results of this computation are given in terms of the following functions:

$$
\begin{aligned}
&g_1(\theta_\vardiamondsuit,\theta_\varheartsuit) := \sqrt{1+\tfrac{z^2}{R^2(\theta_\vardiamondsuit)}}\\
&g_2(\theta_\vardiamondsuit,\theta_\varheartsuit) := \sqrt{1+\tfrac{z^2}{R^2(\theta_\varheartsuit)}}\\
&g_3(\theta_\vardiamondsuit,\theta_\varheartsuit) :\\
&\quad = \tfrac{1}{2}\log\left(\tfrac{(g_1(\theta_\vardiamondsuit,\theta_\varheartsuit)+\cos(\theta_\vardiamondsuit+\beta))(g_2(\theta_\vardiamondsuit,\theta_\varheartsuit)-\cos(\theta_\varheartsuit+\beta))}{(g_1(\theta_\vardiamondsuit,\theta_\varheartsuit)-\cos(\theta_\vardiamondsuit+\beta))(g_2(\theta_\vardiamondsuit,\theta_\varheartsuit)+\cos(\theta_\varheartsuit+\beta))}\right)\\
&g_4(\theta_\vardiamondsuit,\theta_\varheartsuit) := \log\left(\frac{R(\theta_\vardiamondsuit)}{z}+\sqrt{1+\frac{R^2(\theta_\vardiamondsuit)}{z^2}}\right)\\
&g_5(\theta_\vardiamondsuit,\theta_\varheartsuit) := \log\left(\frac{R(\theta_\varheartsuit)}{z}+\sqrt{1+\frac{R^2(\theta_\varheartsuit)}{z^2}}\right)\\
&g_6(\theta_\vardiamondsuit,\theta_\varheartsuit) := \pi - \operatorname{acos}\left(-\tfrac{z\cos(\theta_\varheartsuit+\beta)}{\sqrt{F^2+z^2}}\right)\\
&\qquad\qquad -\operatorname{acos}\left(\tfrac{z\cos(\theta_\vardiamondsuit+\beta)}{\sqrt{F^2+z^2}}\right)\\
&g_7(\theta_\vardiamondsuit,\theta_\varheartsuit) := \tfrac{F^2}{F^2+z^2}.
\end{aligned}
$$

When $z > 0$, the analytical integration over the domain $\mathcal{H}$ yields

$$
I_1^{\mathcal{H}} = \widetilde{K}_{1,1}^{1,1}(\rho_\clubsuit;\theta_\vardiamondsuit,\theta_\varheartsuit) \quad\text{and}\quad I_4^{\mathcal{H}} = \widetilde{K}_{1,3}^{1,1}(\rho_\clubsuit;\theta_\vardiamondsuit,\theta_\varheartsuit),
$$

where

$$
\begin{aligned}
&\widetilde{K}_{1,1}^{1,1}(\rho_\clubsuit;\theta_\vardiamondsuit,\theta_\varheartsuit)\\
&\quad := F g_3(\theta_\vardiamondsuit,\theta_\varheartsuit) + z g_6(\theta_\vardiamondsuit,\theta_\varheartsuit) - (\theta_\varheartsuit-\theta_\vardiamondsuit)\sqrt{\rho_\clubsuit^2+z^2}\\
&\quad \widetilde{K}_{1,3}^{1,1}(\rho_\clubsuit;\theta_\vardiamondsuit,\theta_\varheartsuit) := -\frac{1}{z} g_6(\theta_\vardiamondsuit,\theta_\varheartsuit) + \frac{\theta_\varheartsuit-\theta_\vardiamondsuit}{\sqrt{\rho_\clubsuit^2+z^2}}.
\end{aligned}
$$

For what concerns the computation of $I_2^{\mathcal{H}}$, we have:

$$
\begin{aligned}
I_2^{\mathcal{H}} = \frac{1}{\sin^2\gamma}&\Big[A_{1i}A_{1j}\widetilde{K}_{3,3}^{1,3}(\rho_\clubsuit;\theta_\vardiamondsuit,\theta_\varheartsuit) + (A_{1i}A_{2j}+A_{2i}A_{1j})\\
&\widetilde{K}_{3,3}^{2,2}(\rho_\clubsuit;\theta_\vardiamondsuit,\theta_\varheartsuit) + A_{2i}A_{2j}\widetilde{K}_{3,3}^{3,1}(\rho_\clubsuit;\theta_\vardiamondsuit,\theta_\varheartsuit)\Big]\\
&+\frac{z}{\sin\gamma}\Big[(A_{1i}A_{3j}+A_{3i}A_{1j})\widetilde{K}_{2,3}^{1,2}(\rho_\clubsuit;\theta_\vardiamondsuit,\theta_\varheartsuit)\\
&+(A_{2i}A_{3j}+A_{3i}A_{2j})\widetilde{K}_{2,3}^{2,1}(\rho_\clubsuit;\theta_\vardiamondsuit,\theta_\varheartsuit)\Big]\\
&+z^2A_{3i}A_{3j}\widetilde{K}_{1,3}^{1,1}(\rho_\clubsuit;\theta_\vardiamondsuit,\theta_\varheartsuit),
\end{aligned}
$$

where:

$$
\begin{aligned}
&\widetilde{K}_{2,3}^{1,2}(\rho_\clubsuit;\theta_\vardiamondsuit,\theta_\varheartsuit) := g_5(\theta_\vardiamondsuit,\theta_\varheartsuit)\cos(\gamma-\theta_\varheartsuit)\\
&\quad - g_4(\theta_\vardiamondsuit,\theta_\varheartsuit)\cos(\gamma-\theta_\vardiamondsuit) - g_3(\theta_\vardiamondsuit,\theta_\varheartsuit)\cos\alpha\\
&\quad + \left[\frac{\rho_\clubsuit}{\sqrt{\rho_\clubsuit^2+z^2}} - \log\left(\frac{\rho_\clubsuit+\sqrt{\rho_\clubsuit^2+z^2}}{z}\right)\right]\\
&\left[\cos(\gamma-\theta_\varheartsuit)-\cos(\gamma-\theta_\vardiamondsuit)\right]\\
&\widetilde{K}_{2,3}^{2,1}(\rho_\clubsuit;\theta_\vardiamondsuit,\theta_\varheartsuit) := -g_5(\theta_\vardiamondsuit,\theta_\varheartsuit)\cos\theta_\varheartsuit\\
&\quad + g_4(\theta_\vardiamondsuit,\theta_\varheartsuit)\cos\theta_\vardiamondsuit - g_3(\theta_\vardiamondsuit,\theta_\varheartsuit)\cos\beta\\
&\quad - \left[\frac{\rho_\clubsuit}{\sqrt{\rho_\clubsuit^2+z^2}} - \log\left(\frac{\rho_\clubsuit+\sqrt{\rho_\clubsuit^2+z^2}}{z}\right)\right](\cos\theta_\varheartsuit-\cos\theta_\vardiamondsuit)\\
&\widetilde{K}_{3,3}^{1,3}(\rho_\clubsuit;\theta_\vardiamondsuit,\theta_\varheartsuit) := F[g_2(\theta_\vardiamondsuit,\theta_\varheartsuit)\cos(\theta_\varheartsuit+\alpha-\gamma)\\
&\quad - g_1(\theta_\vardiamondsuit,\theta_\varheartsuit)\cos(\theta_\vardiamondsuit+\alpha-\gamma) + g_3(\theta_\vardiamondsuit,\theta_\varheartsuit)\sin^2\alpha]\\
&\quad + z g_6(\theta_\vardiamondsuit,\theta_\varheartsuit) - \frac{\rho_\clubsuit^2+2z^2}{\sqrt{\rho_\clubsuit^2+z^2}}\Theta_{1,3}(\theta_\vardiamondsuit,\theta_\varheartsuit)\\
&\widetilde{K}_{3,3}^{2,2}(\rho_\clubsuit;\theta_\vardiamondsuit,\theta_\varheartsuit) := F[g_1(\theta_\vardiamondsuit,\theta_\varheartsuit)\cos(\theta_\vardiamondsuit+\alpha) - g_2(\theta_\vardiamondsuit,\theta_\varheartsuit)\\
&\quad \cos(\theta_\varheartsuit+\alpha) - g_3(\theta_\vardiamondsuit,\theta_\varheartsuit)\sin\alpha\sin\beta]\\
&\quad - z g_6(\theta_\vardiamondsuit,\theta_\varheartsuit)\cos\gamma - \frac{\rho_\clubsuit^2+2z^2}{\sqrt{\rho_\clubsuit^2+z^2}}\Theta_{2,2}(\theta_\vardiamondsuit,\theta_\varheartsuit)\\
&\widetilde{K}_{3,3}^{3,1}(\rho_\clubsuit;\theta_\vardiamondsuit,\theta_\varheartsuit) := F[g_1(\theta_\vardiamondsuit,\theta_\varheartsuit)\cos(\theta_\vardiamondsuit-\beta)\\
&\quad - g_2(\theta_\vardiamondsuit,\theta_\varheartsuit)\cos(\theta_\varheartsuit-\beta) + g_3(\theta_\vardiamondsuit,\theta_\varheartsuit)\sin^2\beta]\\
&\quad + z g_6(\theta_\vardiamondsuit,\theta_\varheartsuit) - \frac{\rho_\clubsuit^2+2z^2}{\sqrt{\rho_\clubsuit^2+z^2}}\Theta_{3,1}(\theta_\vardiamondsuit,\theta_\varheartsuit).
\end{aligned}
$$

Finally,

$$
\begin{aligned}
I_3^{\mathcal{H}} = \frac{1}{\sin^2\gamma}&\Big[A_{1i}A_{1j}\widetilde{K}_{3,5}^{1,3}(\rho_\clubsuit;\theta_\vardiamondsuit,\theta_\varheartsuit)\\
&+(A_{1i}A_{2j}+A_{2i}A_{1j})\widetilde{K}_{3,5}^{2,2}(\rho_\clubsuit;\theta_\vardiamondsuit,\theta_\varheartsuit)\\
&+A_{2i}A_{2j}\widetilde{K}_{3,5}^{3,1}(\rho_\clubsuit;\theta_\vardiamondsuit,\theta_\varheartsuit)\Big]\\
&+\frac{z}{\sin\gamma}\Big[(A_{1i}A_{3j}+A_{3i}A_{1j})\widetilde{K}_{2,5}^{1,2}(\rho_\clubsuit;\theta_\vardiamondsuit,\theta_\varheartsuit)\\
&+(A_{2i}A_{3j}+A_{3i}A_{2j})\widetilde{K}_{2,5}^{2,1}(\rho_\clubsuit;\theta_\vardiamondsuit,\theta_\varheartsuit)\Big]\\
&+z^2A_{3i}A_{3j}\widetilde{K}_{1,5}^{1,1}(\rho_\clubsuit;\theta_\vardiamondsuit,\theta_\varheartsuit).
\end{aligned}
$$

where

$$
\begin{aligned}
&\widetilde{K}_{1,5}^{1,1}(\rho_\clubsuit;\theta_\vardiamondsuit,\theta_\varheartsuit) := -\frac{1}{3z^2}\frac{F}{F^2+z^2}\\
&\left[\frac{\cos(\theta_\varheartsuit+\beta)}{g_2(\theta_\vardiamondsuit,\theta_\varheartsuit)} - \frac{\cos(\theta_\vardiamondsuit+\beta)}{g_1(\theta_\vardiamondsuit,\theta_\varheartsuit)}\right]\\
&-\frac{g_6(\theta_\vardiamondsuit,\theta_\varheartsuit)}{3z^3} + \frac{\theta_\varheartsuit-\theta_\vardiamondsuit}{3\left(\rho_\clubsuit^2+z^2\right)^{3/2}}\\
&\widetilde{K}_{2,5}^{1,2}(\rho_\clubsuit;\theta_\vardiamondsuit,\theta_\varheartsuit) := -\frac{\rho_\clubsuit^3}{3z^2(\rho_\clubsuit^2+z^2)^{3/2}}\Theta_{1,2}(\theta_\vardiamondsuit,\theta_\varheartsuit)\\
&\quad + \frac{1}{3z^2}\left[\frac{\sin\alpha\sin(\theta_\varheartsuit+\beta) - g_7(\theta_\vardiamondsuit,\theta_\varheartsuit)\cos\alpha\cos(\theta_\varheartsuit+\beta)}{g_2(\theta_\vardiamondsuit,\theta_\varheartsuit)}\right.
\end{aligned}
$$

Journal: 466 MS: 2312 ☐ TYPESET ☐ DISK ☐ LE ☐ CP Disp.:2023/3/30 Pages: 21 Layout: Large

$$+\frac{g_7(\theta_{\blacklozenge},\theta_{\heartsuit})\cos\alpha\cos\left(\theta_{\blacklozenge}+\beta\right)-\sin\alpha\sin\left(\theta_{\blacklozenge}+\beta\right)}{g_1(\theta_{\blacklozenge},\theta_{\heartsuit})}\Bigg]$$

$$\widetilde{K}^{2,1}_{2,5}(\rho_{\clubsuit};\theta_{\blacklozenge},\theta_{\heartsuit}):=-\frac{\rho_{\clubsuit}^3}{3z^2(\rho_{\clubsuit}^2+z^2)^{3/2}}\Theta_{2,1}(\theta_{\blacklozenge},\theta_{\heartsuit})$$

$$+\frac{1}{3z^2}\Bigg[\frac{\sin\beta\sin\left(\theta_{\blacklozenge}+\beta\right)+g_7(\theta_{\blacklozenge},\theta_{\heartsuit})\cos\beta\cos\left(\theta_{\blacklozenge}+\beta\right)}{g_1(\theta_{\blacklozenge},\theta_{\heartsuit})}+$$

$$-\frac{\sin\beta\sin\left(\theta_{\heartsuit}+\beta\right)+g_7(\theta_{\blacklozenge},\theta_{\heartsuit})\cos\beta\cos\left(\theta_{\heartsuit}+\beta\right)}{g_2(\theta_{\blacklozenge},\theta_{\heartsuit})}\Bigg]$$

$$\widetilde{K}^{1,3}_{3,5}(\rho_{\clubsuit};\theta_{\blacklozenge},\theta_{\heartsuit}):=\frac{3\rho_{\clubsuit}^2+2z^2}{3(\rho_{\clubsuit}^2+z^2)^{3/2}}\Theta_{1,3}(\theta_{\blacklozenge},\theta_{\heartsuit})$$

$$-\frac{g_6(\theta_{\blacklozenge},\theta_{\heartsuit})}{3z}$$

$$+\frac{g_7(\theta_{\blacklozenge},\theta_{\heartsuit})\cos^2\alpha\cos\left(\theta_{\heartsuit}+\beta\right)-\cos\left(\theta_{\heartsuit}+\alpha-\gamma\right)\sin^2\left(\theta_{\heartsuit}+\beta\right)}{3Fg_2(\theta_{\blacklozenge},\theta_{\heartsuit})}$$

$$-\frac{g_7(\theta_{\blacklozenge},\theta_{\heartsuit})\cos^2\alpha\cos\left(\theta_{\blacklozenge}+\beta\right)-\cos\left(\theta_{\blacklozenge}+\alpha-\gamma\right)\sin^2\left(\theta_{\blacklozenge}+\beta\right)}{3Fg_1(\theta_{\blacklozenge},\theta_{\heartsuit})}$$

$$\widetilde{K}^{2,2}_{3,5}(\rho_{\clubsuit};\theta_{\blacklozenge},\theta_{\heartsuit}):=\frac{3\rho_{\clubsuit}^2+2z^2}{3(\rho_{\clubsuit}^2+z^2)^{3/2}}\Theta_{2,2}(\theta_{\blacklozenge},\theta_{\heartsuit})$$

$$+\frac{g_6(\theta_{\blacklozenge},\theta_{\heartsuit})}{3z}\cos\gamma$$

$$+\frac{g_7(\theta_{\blacklozenge},\theta_{\heartsuit})\cos\alpha\cos\beta\cos\left(\theta_{\heartsuit}+\beta\right)+\cos\left(\theta_{\heartsuit}+\alpha\right)\sin^2\left(\theta_{\heartsuit}+\beta\right)}{3Fg_2(\theta_{\blacklozenge},\theta_{\heartsuit})}$$

$$-\frac{g_7(\theta_{\blacklozenge},\theta_{\heartsuit})\cos\alpha\cos\beta\cos\left(\theta_{\blacklozenge}+\beta\right)+\cos\left(\theta_{\blacklozenge}+\alpha\right)\sin^2\left(\theta_{\blacklozenge}+\beta\right)}{3Fg_1(\theta_{\blacklozenge},\theta_{\heartsuit})}$$

$$\widetilde{K}^{3,1}_{3,5}(\rho_{\clubsuit};\theta_{\blacklozenge},\theta_{\heartsuit}):=\frac{3\rho_{\clubsuit}^2+2z^2}{3(\rho_{\clubsuit}^2+z^2)^{3/2}}\Theta_{3,1}(\theta_{\blacklozenge},\theta_{\heartsuit})-\frac{g_6(\theta_{\blacklozenge},\theta_{\heartsuit})}{3z}$$

$$+\frac{g_7(\theta_{\blacklozenge},\theta_{\heartsuit})\cos^2\beta\cos\left(\theta_{\heartsuit}+\beta\right)+\cos\left(\theta_{\heartsuit}-\beta\right)\sin^2\left(\theta_{\heartsuit}+\beta\right)}{3Fg_2(\theta_{\blacklozenge},\theta_{\heartsuit})}$$

$$-\frac{g_7(\theta_{\blacklozenge},\theta_{\heartsuit})\cos^2\beta\cos\left(\theta_{\blacklozenge}+\beta\right)+\cos\left(\theta_{\blacklozenge}-\beta\right)\sin^2\left(\theta_{\blacklozenge}+\beta\right)}{3Fg_1(\theta_{\blacklozenge},\theta_{\heartsuit})}.$$

Remark The values $\widetilde{K}^{h,k}_{i,j}(\theta_{\blacklozenge},\theta_{\heartsuit}):=\widetilde{K}^{h,k}_{i,j}(0;\theta_{\blacklozenge},\theta_{\heartsuit})$, for $i=j=1$ or $i=1,2,3$ and $j=3,5$, are collected in Appendix B. We point out that these functions are involved in the computation of the integral over the domain $\mathcal{G}$.

Remark When the source and the field triangles are in the same plane, i.e. $z=0$, we introduce the function

$$g(\theta_{\blacklozenge},\theta_{\heartsuit}):=\frac{1}{2}\log\left(\frac{(1+\cos\left(\theta_{\blacklozenge}+\beta\right))(1-\cos\left(\theta_{\heartsuit}+\beta\right))}{(1-\cos\left(\theta_{\blacklozenge}+\beta\right))(1+\cos\left(\theta_{\heartsuit}+\beta\right))}\right)$$

and we consider:

$$I_1^{\mathcal{H}}=\overline{K}^{1,1}_{1,1}(\rho_{\clubsuit};\theta_{\blacklozenge},\theta_{\heartsuit})\quad\text{and}\quad I_4^{\mathcal{H}}=\overline{K}^{1,1}_{1,3}(\rho_{\clubsuit};\theta_{\blacklozenge},\theta_{\heartsuit}),$$

where

$$\overline{K}^{1,1}_{1,1}(\rho_{\clubsuit};\theta_{\blacklozenge},\theta_{\heartsuit}):=Fg(\theta_{\blacklozenge},\theta_{\heartsuit})-\rho_{\clubsuit}(\theta_{\heartsuit}-\theta_{\blacklozenge})$$

$$\overline{K}^{1,1}_{1,3}(\rho_{\clubsuit};\theta_{\blacklozenge},\theta_{\heartsuit})$$

$$:=\frac{1}{F}\left[\cos\left(\theta_{\heartsuit}+\beta\right)-\cos\left(\theta_{\blacklozenge}+\beta\right)\right]+\frac{\theta_{\heartsuit}-\theta_{\blacklozenge}}{\rho_{\clubsuit}}.$$

The value of $I_2^{\mathcal{H}}$ is given by the following relationship:

$$I_2^{\mathcal{H}}=\frac{1}{\sin^2\gamma}\Big[A_{1i}A_{1j}\overline{K}^{1,3}_{3,3}(\rho_{\clubsuit};\theta_{\blacklozenge},\theta_{\heartsuit})$$

$$+(A_{1i}A_{2j}+A_{2i}A_{1j})\overline{K}^{2,2}_{3,3}(\rho_{\clubsuit};\theta_{\blacklozenge},\theta_{\heartsuit})$$

$$+A_{2i}A_{2j}\overline{K}^{3,1}_{3,3}(\rho_{\clubsuit};\theta_{\blacklozenge},\theta_{\heartsuit})\Big]$$

where

$$\overline{K}^{1,3}_{3,3}(\rho_{\clubsuit};\theta_{\blacklozenge},\theta_{\heartsuit})$$

$$:=F[g(\theta_{\blacklozenge},\theta_{\heartsuit})\sin^2\alpha+\cos\left(\theta_{\heartsuit}+\alpha-\gamma\right)$$

$$-\cos\left(\theta_{\blacklozenge}+\alpha-\gamma\right)]$$

$$-\rho_{\clubsuit}\Theta_{1,3}(\theta_{\blacklozenge},\theta_{\heartsuit})$$

$$\overline{K}^{2,2}_{3,3}(\rho_{\clubsuit};\theta_{\blacklozenge},\theta_{\heartsuit})$$

$$:=F[\cos\left(\theta_{\blacklozenge}+\alpha\right)-\cos\left(\theta_{\heartsuit}+\alpha\right)-g(\theta_{\blacklozenge},\theta_{\heartsuit})\sin\alpha\sin\beta]$$

$$-\rho_{\clubsuit}\Theta_{2,2}(\theta_{\blacklozenge},\theta_{\heartsuit})$$

$$\overline{K}^{3,1}_{3,3}(\rho_{\clubsuit};\theta_{\blacklozenge},\theta_{\heartsuit})$$

$$:=F[\cos\left(\theta_{\blacklozenge}-\beta\right)-\cos\left(\theta_{\heartsuit}-\beta\right)$$

$$+g(\theta_{\blacklozenge},\theta_{\heartsuit})\sin^2\beta]$$

$$-\rho_{\clubsuit}\Theta_{3,1}(\theta_{\blacklozenge},\theta_{\heartsuit}).$$

Finally, the computation of $I_3^{\mathcal{H}}$ yields

$$I_3^{\mathcal{H}}=\frac{1}{\sin^2\gamma}$$

$$\Big[A_{1i}A_{1j}\overline{K}^{1,3}_{3,5}(\rho_{\clubsuit};\theta_{\blacklozenge},\theta_{\heartsuit})+(A_{1i}A_{2j}+A_{2i}A_{1j})\overline{K}^{2,2}_{3,5}(\rho_{\clubsuit};$$

$$\theta_{\blacklozenge},\theta_{\heartsuit})+A_{2i}A_{2j}\overline{K}^{3,1}_{3,5}(\rho_{\clubsuit};\theta_{\blacklozenge},\theta_{\heartsuit})\Big]$$

Journal: 466 MS: 2312 TYPESET DISK LE CP Disp.:2023/3/30 Pages: 21 Layout: Large

where

$$
\begin{aligned}
&\overline{K}^{1,3}_{3,5}(\rho_{\clubsuit};\theta_{\spadesuit},\theta_{\heartsuit}) := \frac{(1+\cos^2\alpha)\cos(\theta_{\heartsuit}+\beta)-\cos(\theta_{\heartsuit}+\alpha-\gamma)\sin^2(\theta_{\heartsuit}+\beta)}{3F}\\
&-\frac{(1+\cos^2\alpha)\cos(\theta_{\spadesuit}+\beta)-\cos(\theta_{\spadesuit}+\alpha-\gamma)\sin^2(\theta_{\spadesuit}+\beta)}{3F}\\
&+\frac{1}{\rho_{\clubsuit}}\Theta_{1,3}(\theta_{\spadesuit},\theta_{\heartsuit})\overline{K}^{2,2}_{3,5}(\rho_{\clubsuit};\theta_{\spadesuit},\theta_{\heartsuit}) := \frac{[\cos\alpha\cos\beta+\cos(\alpha+\beta)]\cos(\theta_{\heartsuit}+\beta)+\cos(\theta_{\heartsuit}+\alpha)\sin^2(\theta_{\heartsuit}+\beta)}{3F}\\
&-\frac{[\cos\alpha\cos\beta+\cos(\alpha+\beta)]\cos(\theta_{\spadesuit}+\beta)+\cos(\theta_{\spadesuit}+\alpha)\sin^2(\theta_{\spadesuit}+\beta)}{3F}+\frac{1}{\rho_{\clubsuit}}\Theta_{2,2}(\theta_{\spadesuit},\theta_{\heartsuit})\overline{K}^{3,1}_{3,5}(\rho_{\clubsuit};\theta_{\spadesuit},\theta_{\heartsuit})\\
&:=\frac{(1+\cos^2\beta)\cos(\theta_{\heartsuit}+\beta)+\cos(\theta_{\heartsuit}-\beta)\sin^2(\theta_{\heartsuit}+\beta)}{3F}-\frac{(1+\cos^2\beta)\cos(\theta_{\spadesuit}+\beta)+\cos(\theta_{\spadesuit}-\beta)\sin^2(\theta_{\spadesuit}+\beta)}{3F}\\
&+\frac{1}{\rho_{\clubsuit}}\Theta_{3,1}(\theta_{\spadesuit},\theta_{\heartsuit}).
\end{aligned}
$$

6 Numerical results

Here, we address three numerical examples to validate the EBEM approach. As recalled in the previous section, double time integrals are performed analytically as well as the inner space integral over the field triangle. On the contrary, the outer space integral over the source element is numerically computed by using M_g-point Gauss-Hammer quadrature rules. The choice of the parameter $M_g \le 12$ has guaranteed the computation of all the involved integrals with a sufficiently high accuracy. Higher values of M_g could be considered, but they would increase the overall computational cost of the method.

For the generation of the partitioning $\mathcal{T}_{\Delta_{\mathbf{x}}}(\Gamma)$, we have used the GMSH software (see [22]). In particular, we have built uniform or quasi-uniform conforming meshes consisting of triangular elements. All the numerical computations have been performed on a cluster with two Intel® XEON® E5-2683v4 CPUs (2.1 GHz clock frequency and 16 cores) by means of parallel MATLAB® codes.

6.1 Error analysis for an elastodynamic problem exterior to a square crack

In this example, we consider a square crack $\Gamma = \{\mathbf{x} = (x_1, x_2, 0) : -0.5 \le x_i \le 0.5,\ i = 1, 2\}$ and the elastodynamic problem defined in $\Omega = \mathbf{R}^3\backslash\Gamma$, equipped by Dirichlet boundary conditions given on Γ. The chosen P, S-velocities are $c_{\mathrm{P}} = 1\,^{m/s}$ and $c_{\mathrm{S}} = 1/\sqrt{2}\,^{m/s}$, the material density is $\varrho = 1^{kg/m^3}$ and the final time is $T = 1\,s$. The boundary datum $\mathbf{g}(\mathbf{x}; t)$ is assigned in such a way that the analytical solution of (3.9) turns out to be $\mathbf{w}(\mathbf{x}; t) = \mathbf{x}\,t$. We consider successive refinements levels of a uniform coarse mesh constituted by 8 equal triangles (lev. 0) covering Γ. Refinements are obtained halving each triangle side, giving meshes as those depicted in Fig. 6. In Table 1 we show the discretization parameters, together with the error evaluated in $L^2(\Gamma \times [0, T])$ norm:

$$
\begin{aligned}
\varepsilon_{L^2(\Gamma\times[0,T])} &:= \|\mathbf{w} - \widetilde{\mathbf{w}}\|_{L^2(\Gamma\times[0,T])}\\
&= \left[\int_\Gamma \int_0^T \|\mathbf{w}(\mathbf{x}; t) - \widetilde{\mathbf{w}}(\mathbf{x}; t)\|^2 \,\mathrm{d}\Gamma_{\mathbf{x}}\,\mathrm{d}t\right]^{1/2}
\end{aligned}
$$

and the Estimated Order of Convergence (EOC). We remark that, here, $\Delta_{\mathbf{x}}$ corresponds to the cathetus length of the uniform mesh elements, while Δ_t has been chosen in a way such that $c_{\mathrm{P}} = \frac{\Delta_{\mathrm{x}}}{\Delta_t}$.

As one can see, the error decays as $O(\Delta_{\mathbf{x}}^{1.5})$. The observed super-convergence could be ascribed to the regularity of the meshes and the smoothness of the solution.

6.2 Longitudinal waves in a bar

To study the behaviour of the proposed method, we will deduce a Dirichlet problem from a classical benchmark for

Table 1 Discretization parameters for different levels of refinement, space–time L^2 error and EOC

	$\Delta_{\mathrm{x}} = c_{\mathrm{P}}\,\Delta t$	$M_{\Delta_{\mathrm{x}}}$	N_{Δ_t}	$\varepsilon_{L^2(\Gamma\times[0,T])}$	EOC
lev. 0	0.50000	8	2	$4.20\,10^{-2}$	–
lev. 1	0.25000	32	4	$1.52\,10^{-2}$	1.47
lev. 2	0.12500	128	8	$5.21\,10^{-3}$	1.54
lev. 3	0.06250	512	16	$1.81\,10^{-3}$	1.52
lev. 4	0.03125	2048	32	$6.65\,10^{-4}$	1.45

Journal: 466 MS: 2312 TYPESET DISK LE CP Disp.:2023/3/30 Pages: 21 Layout: Large

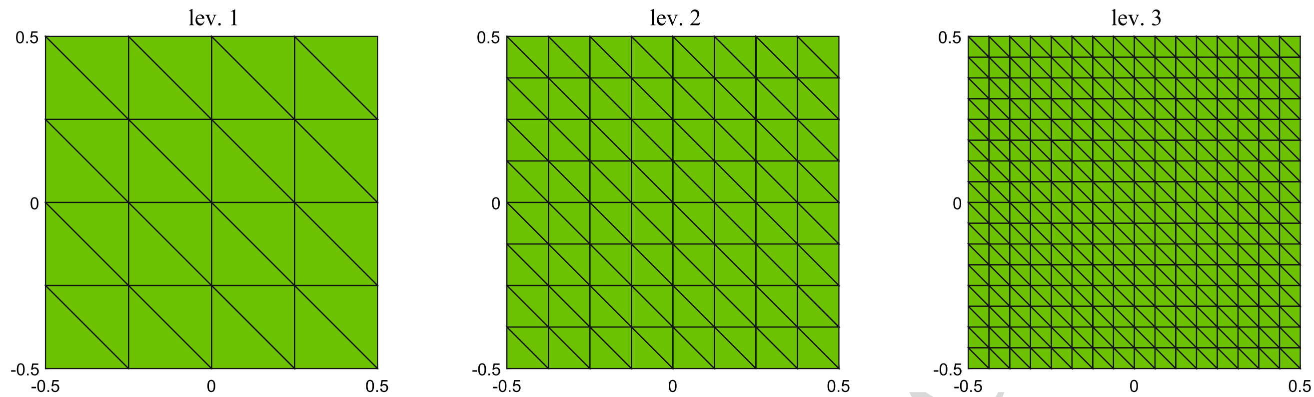

Fig. 6 Meshes on the square crack for successive refinement levels

time-domain BEMs applied to 3D elstodynamics, which is well known to be extremely challenging for what concern standard BEMs analysis in terms of stability properties.

Let us consider a bar Ω_i of height equal to L and square cross section with unit side, depicted in Fig. 7. In literature, this domain is typically equipped with mixed boundary conditions: on the lower surface the Dirichlet boundary datum $\bar{\mathbf{u}}(\mathbf{x};t) = (0,0,0)^\top$ is enforced, while the upper surface is subjected to a uniform normal traction $\bar{\mathbf{p}}(\mathbf{x};t) = (0,0,p_0 H(t))^\top$. On the remaining boundary the tractions are set to zero.

If we set a (artificially) vanishing Poisson's ratio and, consequently $c_\mathrm{P} = \sqrt{2} c_\mathrm{S}$, the related elastodynamic problem possesses an analytical solution, representing the total displacement field in the whole 3D bar volume and surface, directed only in x_3-direction and whose expression coincides with that of the longitudinal waves in a 1D elastodynamic rod (see [21], page 473), i.e.:

$$
\begin{aligned}
u(x;t) = {} & \frac{p_0 H(t)}{\varrho c_\mathrm{P}^2} \sum_{k=0}^{\left\lceil \frac{c_\mathrm{P} T}{2L} \right\rceil - 1} (-1)^k \\
& \left[(c_\mathrm{P} t - 2kL - (L-x)) \right. \\
& H\left(\frac{c_\mathrm{P} t - 2kL - (L-x)}{c_\mathrm{P}} \right) \\
& - (c_\mathrm{P} t - 2(k+1)L + (L-x)) \\
& \left. \times\, H\left(\frac{c_\mathrm{P} t - 2(k+1)L + (L-x)}{c_\mathrm{P}} \right) \right],
\end{aligned}
\qquad (6.1)
$$

Here, we consider problem (2.1), where $\Omega_i = [-l,l]^2 \times [0,L]$, with $l = \frac{1}{2}m$, $L = 3m$. The material parameters $\varrho = 1^{kg/m^3}$ and $\mu = \frac{1}{2}^{kg/ms^2}$ are taken, while we set $p_0 = 1^{kg/ms^2}$, so that $p_0/\varrho c_\mathrm{P}^2 = 1$. Using (6.1), on the boundary Γ of the bar we prescribe the Dirichlet condition:

$$
\mathbf{g}(\mathbf{x};t) = (0,0,u(x_3;t))^\top, \qquad \mathbf{x} \in \Gamma,\ t \in [0,T] \qquad (6.2)
$$

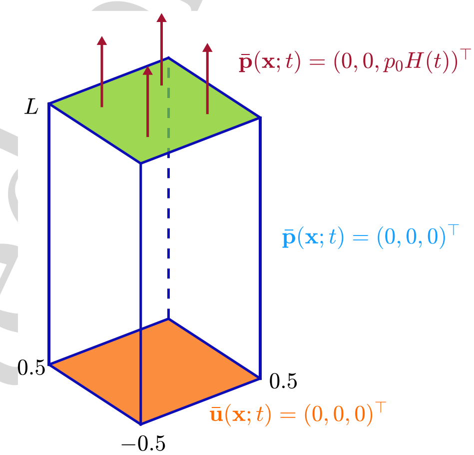

Fig. 7 Bar geometry and boundary conditions typically prescribed in literature

where the overall analyzed time is $T = 36s$. To develop a convergence analysis, we start by considering the coarse mesh associated to the zero level of refinement (lev. 0) and all the successive refinements are obtained by halving each side of its elements. In Fig. 8, the uniform meshes corresponding to the four levels of refinement are represented. In Table 2, the space and time discretization parameters are reported. We remark that, here, $\Delta_\mathbf{x}$ corresponds to the cathetus length of the uniform mesh elements, while Δ_t has been chosen in a way such that $c_\mathrm{P} = \frac{\Delta_\mathbf{x}}{\Delta_t}$. Furthermore, the last column of Table 2 collects the values of the parameter N^* in (4.11), responsible for the reduction of the cost of the proposed approach in terms of memory and computation time. Indeed, we recall that $\mathbb{E}^{(\ell)} = 0$ for $\ell = N^*, \ldots, N_{\Delta_t} - 1$.

In Fig. 9, we show in relation to the finest mesh the whole time history of the third component of the recovered density $\widetilde{w}_3(\mathbf{x};t)$ at the points $\mathbf{x}_0 = (0,0,0)$ (on the bottom face) and $\mathbf{x}_6 = (0,0,3)$ (on the top face), since the components in the x_1- and x_2-directions of the density $\widetilde{\mathbf{w}}(\mathbf{x};t)$ are both trivial. We remark that the oscillations in these plots are clearly asso-

Journal: **466** MS: **2312** ☐ TYPESET ☐ DISK ☐ LE ☐ CP Disp.:**2023/3/30** Pages: **21** Layout: **Large**

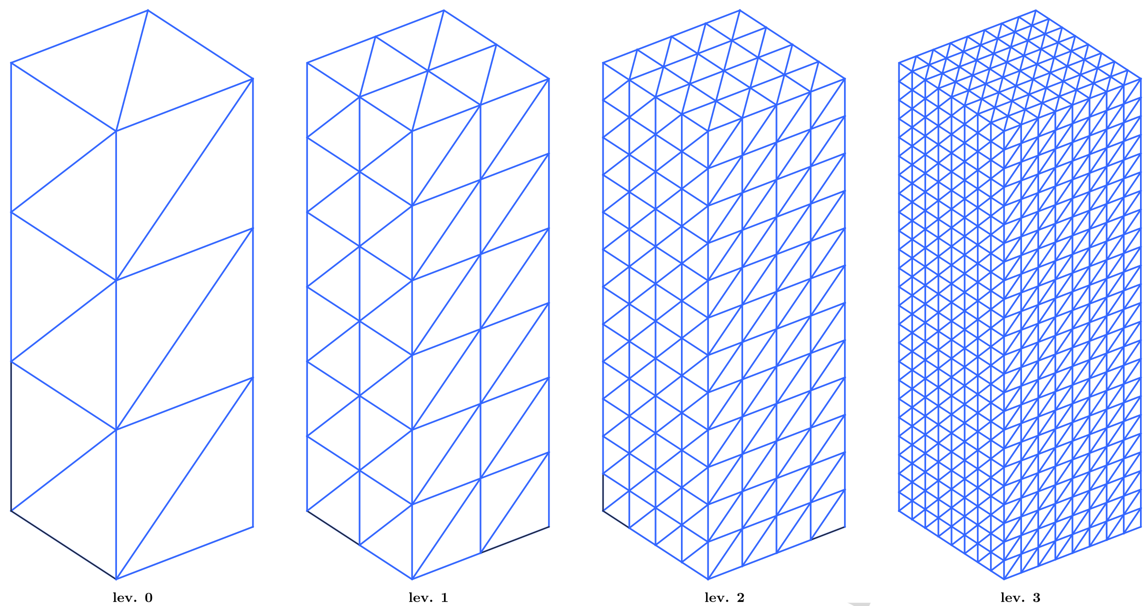

Fig. 8 Meshes of the domain Ω_i for four successive levels of refinement

Table 2 Discretization parameters for different levels of refinement of the bar boundary mesh

	Δ_{x}	$M_{\Delta_{\mathrm{x}}}$	Δ_t	N_{Δ_t}	N^*
lev. 0	1.0000	28	1.0000	36	10
lev. 1	0.5000	112	0.5000	72	14
lev. 2	0.2500	448	0.2500	144	24
lev. 3	0.1250	1792	0.1250	288	42

ciated with the jump discontinuities of the analytical solution, but anyway they remain stable.

To reconstruct the solution of the elastodynamic problem $\mathbf{u}(\mathbf{x};t) = (0,0,u(x_3;t))$, $\mathbf{x} \in \Omega_i$, we plug the computed density $\widetilde{\mathbf{w}}(\mathbf{x};t)$ into the relationship (3.1), obtaining $\widetilde{\mathbf{u}}(\mathbf{x};t)$. The analytical behaviour of the time history of $\mathbf{u}$ is well captured by the third component of $\widetilde{\mathbf{u}}$ (the only one not trivial) for every choice of Δ_{x}, Δ_t presented in Table 2, in particular for the smallest discretization parameters, as it is shown in Fig. 10, where for the highest levels of refinement the recovered displacement $\widetilde{\mathbf{u}}$ in $\mathbf{x}_4 = (0,0,2)$ is indistinguishable from the exact one. This good approximation property is clearly visible also in Fig. 11, where only for $\Delta_{\mathrm{x}} = \Delta_t = 0.125$, the picture on the left presents the whole time history of the recovered displacement field, computed at one of the points, namely $\mathbf{x}_6$, of the upper surface compared to the exact one, while on the right, the behaviour of $\widetilde{u}_3$ at the points $\mathbf{x}_j = (0,0,{}^{j/2})$, for $j = 0,1,2,3,4,5,6$ (placed along a vertical line in the center of the bar) is highlighted.

In order to test the accuracy of the numerical solution retrieved by applying the proposed energetic BEM approach, in Fig. 12, we show the behaviour of the $L^2([0,T])$ absolute error in the point $\mathbf{x}_4$:

$$\varepsilon(\mathbf{x}_4) := \|\widetilde{u}_3(\mathbf{x}_4;\cdot) - u(2;\cdot)\|_{L^2([0,T])}$$

$$= \sqrt{\int_0^T |\widetilde{u}_3(\mathbf{x}_4;t) - u(2;t)|^2 \, \mathrm{d}t}.$$

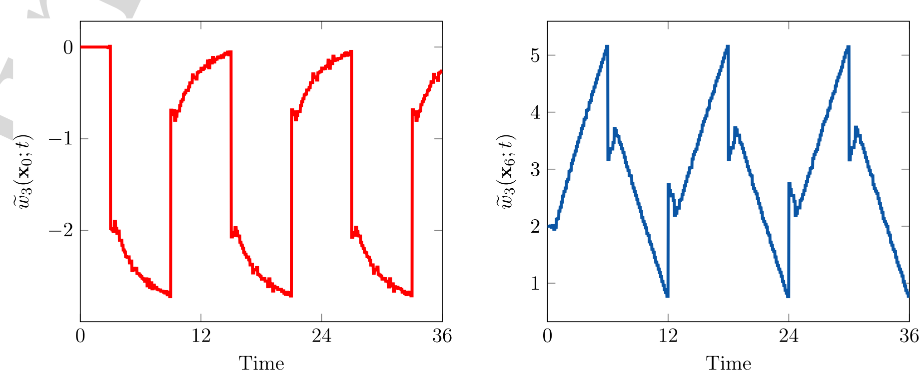

Fig. 9 For $\Delta_t = 0.125$, time history of the component in x_3-direction of the approximated density $\widetilde{\mathbf{w}}$ at the location $\mathbf{x}_0 = (0,0,0)$, on the left, and $\mathbf{x}_6 = (0,0,3)$, on the right

Journal: **466** MS: **2312** ☐ TYPESET ☐ DISK ☐ LE ☐ CP Disp.:**2023/3/30** Pages: **21** Layout: **Large**

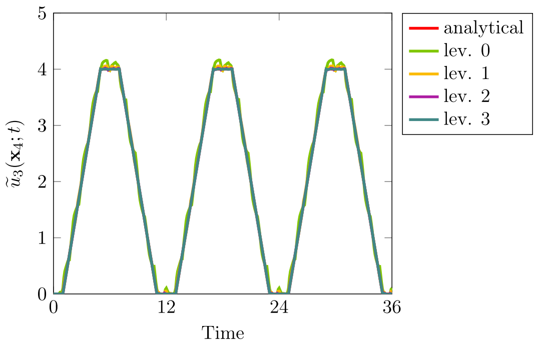

Fig. 10 Time history of the component in x_3-direction of the approximated displacement field $\tilde{\mathbf{u}}$ in $\mathbf{x}_4 = (0, 0, 2)$, recovered for different values of discretization parameters and compared to the analytical one

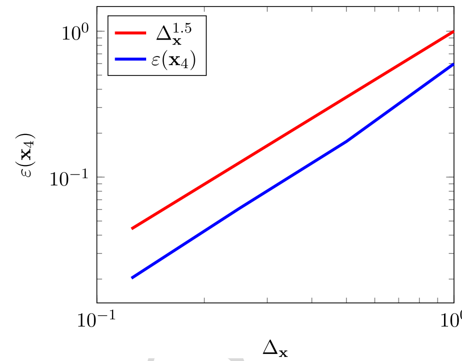

Fig. 12 $L^2([0, T])$ absolute error $\varepsilon(\mathbf{x}_4)$ for the sequence of time and space discretizations described in Table 2

We point out that these results seem to suggest that $\varepsilon(\mathbf{x}_4)$ decays as $O(\Delta_{\mathbf{x}}^{1.5})$. In our numerical experiments, we have observed similar errors when we reconstruct $\tilde{\mathbf{u}}(\mathbf{x}; t)$ in other points $\mathbf{x} \in \Omega_i$.

6.3 Scattering of an incident plane P-wave by the unit sphere

Finally, we consider the problem of scattering by a sphere, which is interesting from the mathematical point of view and has several applications, as reviewed in [30], ranging from acoustics to elastodynamics (see also [32]) and electromagnetism.

Problem (2.1) is here defined in the domain $\Omega_e := \{\mathbf{x} \in \mathbf{R}^3 \;\; x_1^2 + x_2^2 + x_3^2 > 1\}$, external to the unit sphere with boundary Γ and centered at the origin of the axes, endowed with homogeneous initial data and Dirichlet datum $\mathbf{g}(\mathbf{x}; t)$ coinciding with the opposite of an incident plane P-wave $\mathbf{u}_{\text{inc}}(\mathbf{x}; t)$ along the obstacle Γ, i.e. $\mathbf{g}(\mathbf{x}; t) = -\mathbf{u}_{\text{inc}}(\mathbf{x}; t)$. In the following, we assume:

$$\mathbf{u}_{\text{inc}}(\mathbf{x}; t) \\ := \left(e^{-20(x_1-2+c_{\text{P}}t-0.475)^2}, 0, 0\right)^\top.$$

The chosen P, S-velocities are $c_{\text{P}} = 2^{m/s}$ and $c_{\text{S}} = 1^{m/s}$, the material density is $\varrho = 1^{kg/m^3}$ and the final time is $T = 12s$.

The total wave field $\mathbf{u}_{\text{tot}}$ is given by the sum of the incident wave $\mathbf{u}_{\text{inc}}$ and the scattered one $\mathbf{u}_{\text{sca}}$, where the latter is reconstructed in a post-processing phase by using the single-layer representation formula (3.1), once the density $\tilde{\mathbf{w}}$ is numerically computed. For the space discretization we choose a quasi-uniform mesh of Γ consisting of $M_{\Delta_{\mathbf{x}}} = 1488$, with $\Delta_{\mathbf{x}} \simeq 0.125$, while the time interval of interest is subdivided into N = 192 subintervals so that $c_{\text{P}} \simeq \frac{\Delta_{\mathbf{x}}}{\Delta_t}$. In this case, we have observed that $N^* = 38$ and consequently the method is extremely fast.

In Figs. 13 and 14, we present several snapshots related to the components in the x_1- and x_2-directions, respectively, of the reconstructed scattered field in the square $[-5, 5] \times [-5, 5]$, laying on the plane $x_3 = 0$ and external to the obstacle, for different time instants. We omit the plot of the component in the x_3-direction because it is trivial. These results show the capability of the proposed method to simulate a complete wavefield since an S-wave appears once the scattered field in x_1-direction, generated by the given Dirichlet datum, bumps against the obstacle and is reflected back.

Conclusion and perspectives

We have considered a boundary integral reformulation of 3D time-domain interior and exterior wave problems, endowed

Fig. 11 For $\Delta_x = 0.125$, $\Delta_t = 0.125$, on the left, time history of the component in x_3-direction of the recovered displacement field $\tilde{\mathbf{u}}$ in $\mathbf{x}_6$ compared with the analytical one and, on the right, evolution of the approximated $\tilde{u}_3$ at different heights along a vertical line in the center of the bar)

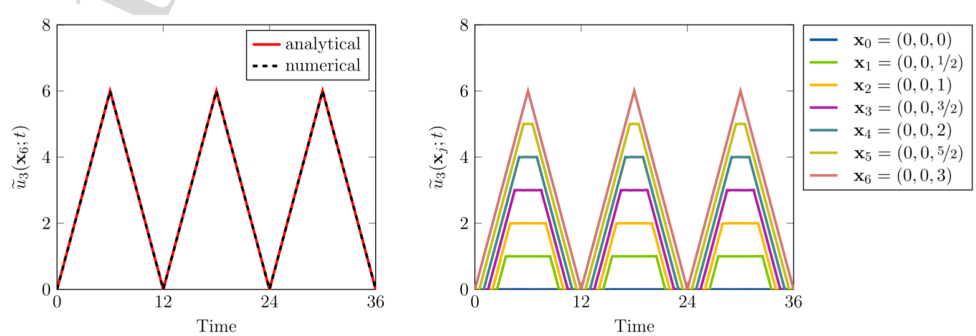

Journal: 466 MS: 2312 TYPESET DISK LE CP Disp.:2023/3/30 Pages: 21 Layout: Large

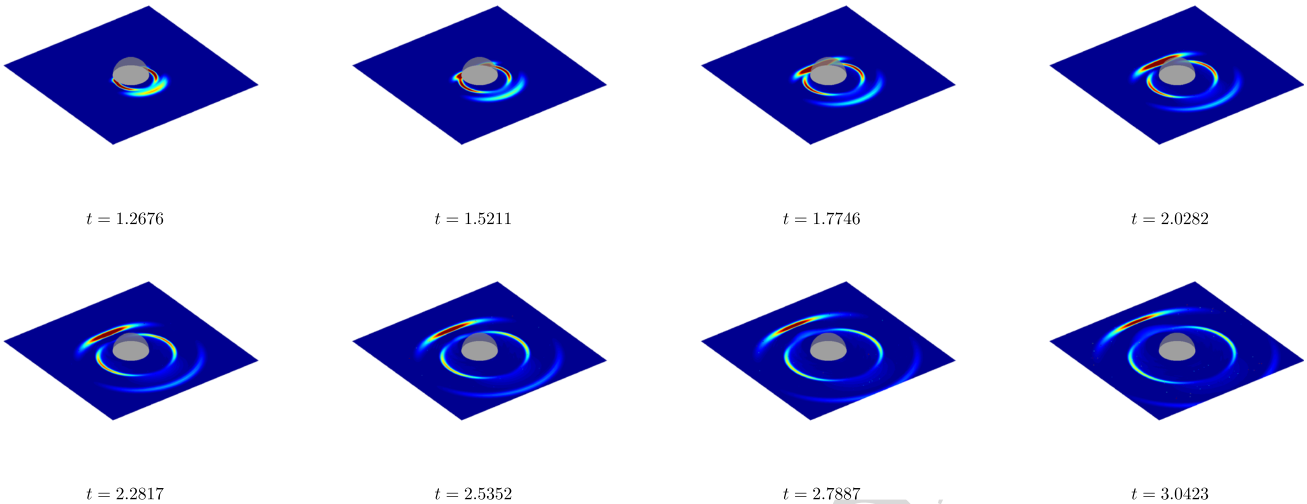

Fig. 13 Scattering of a plane incident P-wave by the unit sphere. Snapshots of the component in the x_1-direction of the reconstructed scattered field $\mathbf{u}_{sca}$ around the obstacle at different time instants

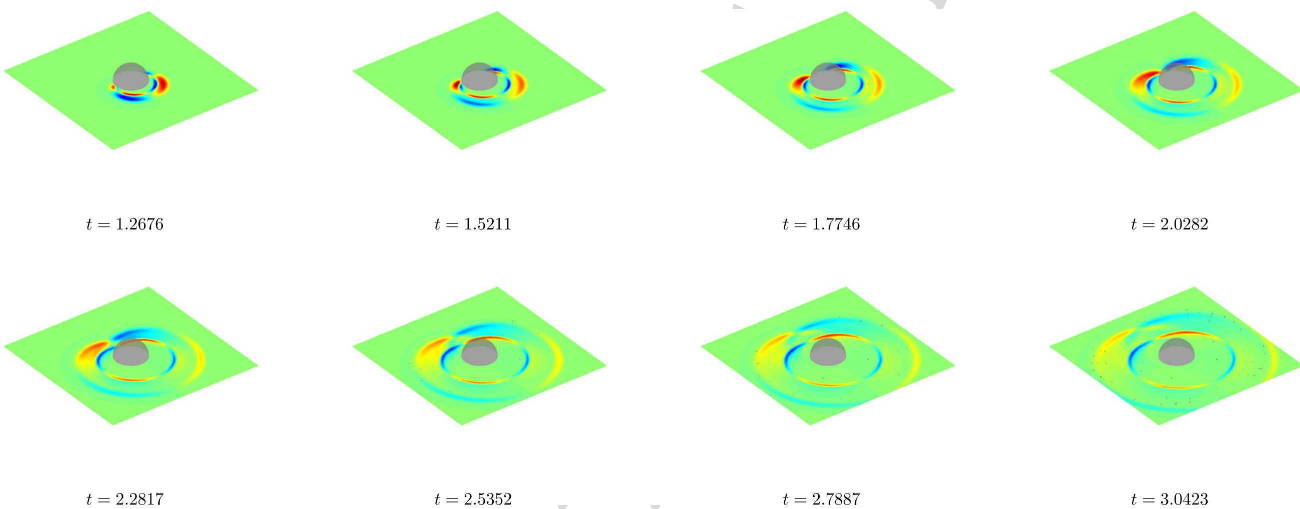

Fig. 14 Scattering of a plane incident P-wave by the unit sphere. Snapshots of the component in the x_2-direction of the reconstructed scattered field $\mathbf{u}_{sca}$ around the obstacle at different time instants

with a Dirichlet type boundary and null initial conditions. For the resolution of the corresponding boundary integral equation, we have used the space–time energetic Galerkin boundary element method with double analytical integration in time variable. The resulting weakly singular double integrals in space variables are then evaluated by inner analytical and outer numerical integrations. This issue has already been encountered and analysed in [5], where the energetic BEM has been applied to solve 3D acoustic (scalar) wave problems. However, the extension of this method to the elastodynamic (vector) case is not trivial, since a rigorous classification of integration domains with shapes strongly dependent on the advancement of P- and S-wave fronts is required. The accurate detection of these domains is essential to avoid computational inaccuracy and to overcome the difficulties entailed by the integration of the Heaviside functions, that model the wave fronts propagation. This issue, as already observed in the context of 2D elastodynamic wave problems (see [11]), is crucial to maintain the global efficiency and stability of the entire energetic procedure. Furthermore, we have theoretically and numerically shown that the computational cost and memory storage required by the proposed numerical method can be significantly reduced by taking into account a cut-off property known since the work of Mansur [28] and used for instance in [25, 26] .

Unfortunately, even if the energetic BEM takes advantage from the dimensionality reduction of the problem, working on the boundary and not on the spatial domain, 3D realistic problems involve a large number of surface degrees of freedom. Therefore, the traditional implementation on ordi-

Journal: 466 MS: 2312 TYPESET DISK LE CP Disp.:2023/3/30 Pages: 21 Layout: Large

nary laptops of the method is prohibitive as soon as the space dimension becomes large, and it is restricted to problems of small size, typically $\mathcal{O}(10^3)$ degrees of freedom, as shown in the presented numerical tests. We remark that at the current stage the design and the implementation of fast, stable and accurate solvers, that allow to increase the capabilities of space–time BEMs, are still open questions (see [12] and [20] for recent developments in 2D). Even if this issue is crucial for successful applications of the proposed method to large scale HPC applications, it is out of the aim of the present pioneering paper. Since these aspects are worth of study, they will be the subject of future investigations. On the other side, the study of Energetic BEM for the more interesting 3D elastodynamic PDE equipped by mixed or Neumann boundary condition is currently taken into account, with the development of space–time double layer potential and hypersingular integral operator discretizations, extending what has been done in [6] for 3D acoustic wave propagation.

Appendix

In the case of acoustic (scalar) wave propagation problems, for a given child triangle $\breve{E}_m^{(k)}$ a single circular wave front induces, in the most general case, a partition represented by (the sum of) a triangle (region $\mathcal{G}$) and two circular sectors (region $\mathcal{E}$). In this Appendix, we detail the analytical inner integration over these two types of domain.

A Results of the analytical integration over a circular sector

We have already remarked that, when $\rho_{\clubsuit} = 0$, the domain $\mathcal{F}$ coincides with $\mathcal{E}$ (circular sector). In this special case, the expression of the functions $K_{i,j}(\rho_{\spadesuit}) := K_{i,j}(0, \rho_{\spadesuit})$, for $i = j = 1$ or $i = 1, 2, 3$ and $j = 3, 5$, simplifies as it follows:

$$K_{1,1}(\rho_{\spadesuit}) := \sqrt{\rho_{\spadesuit}^2 + z^2} - z$$

$$K_{1,3}(\rho_{\spadesuit}) := -\frac{1}{\sqrt{\rho_{\spadesuit}^2 + z^2}} + \frac{1}{z}$$

$$K_{1,5}(\rho_{\spadesuit}) := \frac{1}{3}\left[\frac{1}{z^3} - \left(\frac{1}{\sqrt{\rho_{\spadesuit}^2 + z^2}}\right)^3\right]$$

$$K_{2,3}(\rho_{\spadesuit}) := \log\left(\frac{\rho_{\spadesuit} + \sqrt{\rho_{\spadesuit}^2 + z^2}}{z}\right) - \frac{\rho_{\spadesuit}}{\sqrt{\rho_{\spadesuit}^2 + z^2}}$$

$$K_{2,5}(\rho_{\spadesuit}) := \frac{1}{3z^2}\left(\frac{\rho_{\spadesuit}}{\sqrt{\rho_{\spadesuit}^2 + z^2}}\right)^3$$

$$K_{3,3}(\rho_{\spadesuit}) := \sqrt{\rho_{\spadesuit}^2 + z^2} + \frac{z^2}{\sqrt{\rho_{\spadesuit}^2 + z^2}} - 2z$$

$$K_{3,5}(\rho_{\spadesuit}) := \frac{2}{3z} - \frac{1}{\sqrt{\rho_{\spadesuit}^2 + z^2}} + \frac{z^2}{3}\left(\frac{1}{\sqrt{\rho_{\spadesuit}^2 + z^2}}\right)^3.$$

Since they depend on z, we point out that in this scenario z is always greater than 0.

B Results of the analytical integration over a triangle

For what concerns the collapsed version of the domain $\mathcal{H}$, i.e. the triangle $\mathcal{G}$, we report here the values of $\widetilde{K}_{i,j}^{h,k}(\theta_{\blacklozenge}, \theta_{\heartsuit}) := \widetilde{K}_{i,j}^{h,k}(0; \theta_{\blacklozenge}, \theta_{\heartsuit})$, where the indices $h, k = 1, 2, 3$ are such that $2 \le h + k < 5$, while the indices i and j are such that $i = j = 1$ or $i = 1, 2, 3$ and $j = 3, 5$. For easiness of the presentation, we collect the expression of $\widetilde{K}_{i,j}^{h,k}(\theta_{\blacklozenge}, \theta_{\heartsuit})$ on the basis of the values of the indices h and k, so that

- for $h = k = 1$ we have:

$$\widetilde{K}_{1,1}^{1,1}(\theta_{\blacklozenge}, \theta_{\heartsuit}) := F g_3(\theta_{\blacklozenge}, \theta_{\heartsuit}) + z g_6(\theta_{\blacklozenge}, \theta_{\heartsuit}) - z(\theta_{\heartsuit} - \theta_{\blacklozenge})$$

$$\widetilde{K}_{1,3}^{1,1}(\theta_{\blacklozenge}, \theta_{\heartsuit}) := -\frac{1}{z} g_6(\theta_{\blacklozenge}, \theta_{\heartsuit}) + \frac{1}{z}(\theta_{\heartsuit} - \theta_{\blacklozenge})$$

$$\widetilde{K}_{1,5}^{1,1}(\theta_{\blacklozenge}, \theta_{\heartsuit}) := -\frac{1}{3z^2}\frac{F}{F^2 + z^2}\left[\frac{\cos(\theta_{\heartsuit} + \beta)}{g_2(\theta_{\blacklozenge}, \theta_{\heartsuit})} - \frac{\cos(\theta_{\blacklozenge} + \beta)}{g_1(\theta_{\blacklozenge}, \theta_{\heartsuit})}\right] - \frac{g_6(\theta_{\blacklozenge}, \theta_{\heartsuit})}{3z^3} + \frac{\theta_{\heartsuit} - \theta_{\blacklozenge}}{3z^3}$$

- for $h = 1$ and $k = 2$ we have

$$\widetilde{K}_{2,3}^{1,2}(\theta_{\blacklozenge}, \theta_{\heartsuit}) := g_5(\theta_{\blacklozenge}, \theta_{\heartsuit})\cos(\gamma - \theta_{\heartsuit}) - g_4(\theta_{\blacklozenge}, \theta_{\heartsuit}) \cos(\gamma - \theta_{\blacklozenge}) - g_3(\theta_{\blacklozenge}, \theta_{\heartsuit})\cos\alpha$$

$$\widetilde{K}_{2,5}^{1,2}(\theta_{\blacklozenge}, \theta_{\heartsuit}) := \frac{1}{3z^2} \times \left[\frac{\sin\alpha\sin(\theta_{\heartsuit} + \beta) - g_7(\theta_{\blacklozenge}, \theta_{\heartsuit})\cos\alpha\cos(\theta_{\heartsuit} + \beta)}{g_2(\theta_{\blacklozenge}, \theta_{\heartsuit})} + \frac{g_7(\theta_{\blacklozenge}, \theta_{\heartsuit})\cos\alpha\cos(\theta_{\blacklozenge} + \beta) - \sin\alpha\sin(\theta_{\blacklozenge} + \beta)}{g_1(\theta_{\blacklozenge}, \theta_{\heartsuit})}\right]$$

Journal: 466 MS: 2312 TYPESET DISK LE CP Disp.:2023/3/30 Pages: 21 Layout: Large

- for $h = 1$ and $k = 3$ we have

$$
\begin{aligned}
\widetilde{K}^{1,3}_{3,3}(\theta_\blacklozenge, \theta_\heartsuit) &:= F[g_2(\theta_\blacklozenge, \theta_\heartsuit)\cos(\theta_\heartsuit + \alpha - \gamma) \\
&- g_1(\theta_\blacklozenge, \theta_\heartsuit)\cos(\theta_\blacklozenge + \alpha - \gamma) + g_3(\theta_\blacklozenge, \theta_\heartsuit)\sin^2\alpha] \\
&+ z g_6(\theta_\blacklozenge, \theta_\heartsuit) - 2z\Theta_{1,3}(\theta_\blacklozenge, \theta_\heartsuit) \\
\widetilde{K}^{1,3}_{3,5}(\theta_\blacklozenge, \theta_\heartsuit) &:= \frac{2}{3z}\Theta_{1,3}(\theta_\blacklozenge, \theta_\heartsuit) - \frac{g_6(\theta_\blacklozenge, \theta_\heartsuit)}{3z} \\
&+ \frac{g_7(\theta_\blacklozenge, \theta_\heartsuit)\cos^2\alpha\cos(\theta_\heartsuit + \beta) - \cos(\theta_\heartsuit + \alpha - \gamma)\sin^2(\theta_\heartsuit + \beta)}{3F g_2(\theta_\blacklozenge, \theta_\heartsuit)} \\
&- \frac{g_7(\theta_\blacklozenge, \theta_\heartsuit)\cos^2\alpha\cos(\theta_\blacklozenge + \beta) - \cos(\theta_\blacklozenge + \alpha - \gamma)\sin^2(\theta_\blacklozenge + \beta)}{3F g_1(\theta_\blacklozenge, \theta_\heartsuit)}
\end{aligned}
$$

- for $h = 2$ and $k = 1$ we have

$$
\begin{aligned}
\widetilde{K}^{2,1}_{2,3}(\theta_\blacklozenge, \theta_\heartsuit) &:= -g_5(\theta_\blacklozenge, \theta_\heartsuit)\cos\theta_\heartsuit + g_4(\theta_\blacklozenge, \theta_\heartsuit)\cos\theta_\blacklozenge \\
&- g_3(\theta_\blacklozenge, \theta_\heartsuit)\cos\beta\,\widetilde{K}^{2,1}_{2,5}(\theta_\blacklozenge, \theta_\heartsuit) := \frac{1}{3z^2} \\
&\times \left[\frac{\sin\beta\sin\left(\theta_\blacklozenge + \beta\right) + g_7(\theta_\blacklozenge, \theta_\heartsuit)\cos\beta\cos\left(\theta_\blacklozenge + \beta\right)}{g_1(\theta_\blacklozenge, \theta_\heartsuit)} + \right. \\
&\left. - \frac{\sin\beta\sin\left(\theta_\heartsuit + \beta\right) + g_7(\theta_\blacklozenge, \theta_\heartsuit)\cos\beta\cos\left(\theta_\heartsuit + \beta\right)}{g_2(\theta_\blacklozenge, \theta_\heartsuit)}\right]
\end{aligned}
$$

- for $h = k = 2$ we have

$$
\begin{aligned}
\widetilde{K}^{2,2}_{3,3}(\theta_\blacklozenge, \theta_\heartsuit) &:= F[g_1(\theta_\blacklozenge, \theta_\heartsuit)\cos(\theta_\blacklozenge + \alpha) \\
&- g_2(\theta_\blacklozenge, \theta_\heartsuit)\cos(\theta_\heartsuit + \alpha) - g_3(\theta_\blacklozenge, \theta_\heartsuit)\sin\alpha\sin\beta] \\
&- z g_6(\theta_\blacklozenge, \theta_\heartsuit)\cos\gamma - 2z\Theta_{2,2}(\theta_\blacklozenge, \theta_\heartsuit)
\end{aligned}
$$

- for $h = 3$ and $k = 1$ we have

$$
\begin{aligned}
\widetilde{K}^{3,1}_{3,3}(\theta_\blacklozenge, \theta_\heartsuit) &:= F[g_1(\theta_\blacklozenge, \theta_\heartsuit)\cos(\theta_\blacklozenge - \beta) \\
&- g_2(\theta_\blacklozenge, \theta_\heartsuit)\cos(\theta_\heartsuit - \beta) + g_3(\theta_\blacklozenge, \theta_\heartsuit)\sin^2\beta] \\
&+ z g_6(\theta_\blacklozenge, \theta_\heartsuit) - 2z\Theta_{3,1}(\theta_\blacklozenge, \theta_\heartsuit).
\end{aligned}
$$

Even in this case, z is always greater than 0.

References

1. Abramowitz M, Stegun I (1964) Handbook of mathematical functions. NBS (1964)
2. Aimi A, Diligenti M (2008) A new space–time energetic formulation for wave propagation analysis in layered media by BEMs. Int J Numer Methods Eng 75(9):1102–1132
3. Aimi A, Diligenti M, Guardasoni C, Mazzieri I, Panizzi S (2009) An energy approach to space–time Galerkin BEM for wave propagation problems. Int J Numer Methods Eng 80(9):1196–1240
4. Aimi A, Diligenti M, Frangi A, Guardasoni C (2012) A stable 3D energetic Galerkin BEM approach for wave propagation interior problems. Eng Anal Bound Elem 36(12):1756–1765
5. Aimi A, Diligenti M, Frangi A, Guardasoni C (2013) Neumann exterior wave propagation problems: computational aspects of 3D energetic Galerkin BEM. Comput Mech 51(4):475–493
6. Aimi A, Diligenti M, Frangi A, Guardasoni C (2014) Energetic BEM-FEM coupling for wave propagation in 3D multidomains. Int J Numer Method Eng 97:377–394
7. Aimi A, Desiderio L, Diligenti M, Guardasoni C (2014) A numerical study of energetic BEM-FEM applied to wave propagation in 2D multidomains. Publications de l'Institut Mathématique 96(110):5–22
8. Aimi A, Desiderio L, Diligenti M, Guardasoni C (2019) Application of energetic BEM to 2D elastodynamic soft scattering problems. Commun Appl Ind Math 10(1):182–198
9. Aimi A, Desiderio L, Fedeli P, Frangi A (2021) A fast boundary-finite element approach for estimating anchor losses in micro-electro-mechanical system resonators. Appl Math Model 97:741–753
10. Aimi A, Di Credico G, Gimperlein H, Stephan EP. Higher-order time domain boundary elements for elastodynamics—graded meshes and hp-versions (under review)
11. Aimi A, Di Credico G, Diligenti M, Guardasoni C (2022) Highly accurate quadrature schemes for singular integrals in energetic BEM applied to elastodynamics. J Comput Appl Math 410:114186
12. Aimi A, Desiderio L, Di Credico G (2022) Partially pivoted ACA based acceleration of the Energetic BEM for time-domain acoustic and elastic waves exterior problems. Comput Math Appl 119:351–370
13. Anderson TG, Bruno OP, Lyon M (2020) High-order, dispersionless "fast-hybrid" wave equation solver. Part I: O(1) sampling cost via incident-field windowing and recentering. SIAM J Sci Comput 42(2):A1348–A1379
14. Bamberger A, Ha Duong T (1986) Formulation variationelle espace-temps pour le calcul par potentiel retardé de la difraction d'une onde acoustique. Math Methods Appl Sci 8:405–435
15. Bonnet M (1995) Boundary integral equation methods for solids and fluids. Wiley, Hoboken
16. Chaillat S, Desiderio L, Ciarlet P Jr (2017) Theory and implementation of $\mathcal{H}$-matrix based iterative and direct solvers for oscillatory kernels. J Comput Phys 351:165–186
17. Chen G, Zhou J (2010) Boundary element methods with applications to nonlinear problems. Atlantis Press, Paris
18. Costabel M (2004) Time-dependent problems with the boundary integral equation method. Encycl Comput Mech 1:703–721
19. Desiderio L (1978) An $\mathcal{H}$-matrix based direct solver for the Boundary Element Method in 3D elastodynamics. AIP Conf Proc 2018:120005
20. Desiderio L, Falletta S (2020) Efficient solution of two-dimensional wave propagation problems by CQ-wavelet BEM: algorithm and applications. SIAM J Sci Comput 42(4):B894–B920
21. Eringen AC, Suhubi ES (1975) Elastodynamics. Academic Press, New York
22. Geuzaine C, Remacle JF (2009) Gmsh: a three-dimensional finite element mesh generator with built-in pre- and post processing facilities. Int J Numer Methods Eng 79:1309–1331
23. Jang HW, Ih JG (2012) Stabilization of time domain acoustic boundary element method for the exterior problem avoiding the nonuniqueness. J Acoust Soc Am 133(3):1237–1244
24. Joly P, Rodriguez J (2017) Mathematical aspects of variational boundary integral equations for time dependent wave propagation. J Integr Equ Appl 29(1):137–187
25. Kager B (2014) Efficient convolution quadrature based boundary element formulation for time-domain elastodynamics. PhD Thesis, Technischen Universitat Graz
26. Kager B, Schanz M (2015) Fast and data sparse time domain BEM for elastodynamics. Eng Anal Bound Elem 50:212–223
27. Lubich C (1994) On the multistep time discretization of linear initial-boundary value problems and their boundary integral equations. Numer Math 67(3):365–389

Journal: 466 MS: 2312 TYPESET DISK LE CP Disp.:2023/3/30 Pages: 21 Layout: Large

28. Mansur WJ (1983) A time-stepping technique to solve wave propagation problems using the boundary element method. PhD thesis, University of Southampton
29. Mansur WJ, Brebbia CA (1985) Further developments on the solution of the transient scalar wave equation. In: Brebbia CA (ed) Topics in boundary elements research 2. Springer, Berlin, pp 87–123
30. Martin PA (2021) Time-domain scattering. Cambridge University Press, Cambridge
31. Milroy J, Hinduja S, Davey K (1997) The elastostatic three-dimensional boundary element method: analytical integration for linear isoparametric triangular elements. Appl Math Model 21:763–782
32. Norwood FR (1967) Diffraction of transient elastic waves by a spherical cavity. Ph.D. Thesis, Caltech
33. Quarteroni A, Valli A (1994) A numerical approximation of partial differential equations. Springer, Berlin
34. Rynne BP (1985) Stability and convergence of time marching methods in scattering problems. IMA J Appl Math 35(3):297–310
35. Schanz M (2018) Fast multipole method for poroelastodynamics. Eng Anal Bound Elem 89:50–59

Journal: **466** MS: **2312** TYPESET DISK LE CP Disp.:**2023/3/30** Pages: **21** Layout: **Large**

Journal: 466
Article: 2312

Author Query Form

Please ensure you fill out your response to the queries raised below and return this form along with your corrections

Dear Author

During the process of typesetting your article, the following queries have arisen. Please check your typeset proof carefully against the queries listed below and mark the necessary changes either directly on the proof/online grid or in the 'Author's response' area provided below

Query	Details required	Author's response
1.	Please check and confirm the edit made in the article title.	
2.	Please check and confirm the inserted city for the affiliations 1 and 2.	
3.	Please provide the complete details for the reference Aimi et al. (under review).	